Concentration effects on optical properties, DFT, crystal characterization and α-glucosidase activity studies: Novel Zn(II) complex

Necmi Dege [a], Özgen Özge [b,1], Davut Avcı [b,*], Adil Başoğlu [b,*], Fatih Sönmez [c], Mavişe Yaman [a], Ömer Tamer [b], Yusuf Atalay [b], Belma Zengin Kurt [d]

[a] Ondokuz Mayıs University, Faculty of Arts and Sciences, Department of Physics, 55139 Samsun, Turkey
[b] Sakarya University, Faculty of Arts and Sciences, Department of Physics, 54187 Sakarya, Turkey
[c] Sakarya University of Applied Sciences, Pamukova Vocational High School, 54055 Sakarya, Turkey
[d] Bezmialem Vakif University, Faculty of Pharmacy, Department of Pharmaceutical Chemistry, 34093 Istanbul, Turkey

HIGHLIGHTS

- Novel Zn(II) complex was synthesized and its crystal structure was determined.
- The experimental optical properties at different concentrations were investigated.
- The IC_{50} value of Zn(II) complex against α-glucosidase was also determined.
- DFT/M06-L and ωB97XD levels were used for spectral and optical properties.
- The experimental and theoretical results were comparatively presented.

GRAPHICAL ABSTRACT
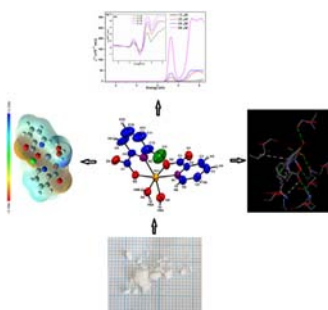
ARTICLE INFO

ABSTRACT

A novel Zn(II) complex of 6-ClpicH and picH was synthesized and its structure was determined by XRD technique. The detailed experimental optical susceptibility and band gap, refractive index, linear polarizability, optical and electrical conductivity parameters in various concentrations were investigated by means of the UV–Vis spectroscopic data. The optical band gap, refractive index (n), linear optical susceptibility ($\chi^{(1)}$), third-order nonlinear optical susceptibility ($\chi^{(3)}$), second- and third-order nonlinear optical (β and γ) parameters were examined by using DFT/M06-L and ωB97XD/6–311++G(d,p) levels. The IC_{50} value of Zn(II) complex against α-glucosidase was also obtained at 0.44 mM. The experimental band gap of the Zn(II) complex at 13, 33, 44 and 94 μM concentrations in ethanol were found to be 4.38, 4.37, 4.35 and 4.28 eV, respectively. The third-order NLO susceptibility $\chi^{(3)}$ parameter at 94 μM concentration corresponding to the photon energies of 4.6 and 5.7 eV in the UV–Vis region were observed at 206.6×10^{-13} and 294.3×10^{-13} esu, respectively. Besides, the theoretical $\chi^{(3)}$ values were obtained at 50.58×10^{-13} and 20.37×10^{-13} esu by using M06-L level. These results indicate that Zn(II) complex could be an effective third-order NLO candidate material. In brief, the detailed theoretical and experimental structural, spectral and optical properties of the Zn(II) complex were presented comparatively.

* Corresponding authors.
  E-mail addresses: davci@sakarya.edu.tr (D. Avcı), abasoglu@sakarya.edu.tr (A. Başoğlu).
  [1] YÖK 100/2000 PhD Scholarship.

1. Introduction

Pyridine-2-carboxylic acid (2-picolinic acid, picH) and its derivatives (6-methyl/6-chloro/6-bromo, 3-methyl/3-hydroxypyridine-2-carboxylic acid, etc.) have an immense interest due to their coordination flexibility with a variety of metal ions [1–16]. These compounds possess pyridine-N and carboxylate-O atom and generally bind to metal via *N* and *O* donor atom forming five member rings. Many complexes of the picolinate-base ligands with metal ions have been examined as models for their wide spectrum of biological activity, such as enzyme activity [17–21] and DNA-cleavage system [13,22,23], etc. Besides these biological activities, interest in these compounds also stems from their various chemical, structural, physicochemical and optical properties.

α-Glucosidase (EC 3.2.1.20), associated with type 2 diabetes mellitus (T2DM), provide the formation of α-glucose at the end of the substrate chain through hydrolyzing terminal glycosidic bonds [17–19]. α-Glucosidase inhibitors (AGI), one of the agents that reduce postprandial hyperglycemia, have an important role in the treatment of T2DM and pre-diabetic conditions in terms of delaying carbohydrate digestion, prolonging the overall carbohydrate digestion period, and slowing glucose absorption. The inhibitory activity of Zn(II) complexes containing picolinate (pa/pic) and its derivatives against α-glucosidase have been reported for Zn (pa)$_2$ [24], Zn(6mpa–ma)$_2$SO$_4$ [25] and [Zn(6-mpa)$_2$(H$_2$O)]·H$_2$O [21]. The influence of these complexes is due to the strong chelating ability of these ligands with biologically important metal ions. Therefore, scientific researches with regard to the design and synthesis of effective glucosidase inhibitors have been continued.

In addition to the structural and spectral characterizations of the metal complexes in the experimental and theoretical studies, the investigations of linear and nonlinear optical features owing to telecommunication technology applications such as information storage, optical switching and communication have a great importance [26–30]. Depending on the technological requirements, the novel optical materials could be afforded due to the versatile metal–ligand bonds of non-centrosymmetric systems in complex crystal structures. While some organic compounds containing the electron-acceptor (A)-π system-electron donor (D)/A-π-D type structures having the high values of first-order hyperpolarizability (β) have been broadly examined [31–35], the metal complex structures have been less investigated because of the centrosymmetric or noncentrosymmetric coordination geometries around the central metal ions playing an effective role for the β value in these structures. The powerful intramolecular charge transfer (ICT) arose from between electron donating and accepting units owing to π-bridge in NLO materials could be stated the large difference between ground and excited dipole moments. Furthermore, the dominant electronic transitions in the metal complex structures appear the NLO response of the electron donating and accepting units around the metal ions acting as π-bridge. These systems not only reduce the frontier orbital energy gap and increase NLO response, but also provide to increase asymmetric electronic distribution and the electronic absorption.

New density functional theory (DFT) models facilitate the elucidation of different structure–property relationships in many different molecular systems. DFT models used commonly are B3LYP, B3PW91, PBE1PBE (the hybrid GGA), M06-2X, M06-L (hybrid meta-GGA), ωB97XD, CAM-B3LYP and LC-ωPBE (long range (LR) corrected hybrid functionals). The ωB97XD method [36] containing the long-range correction with empirical atom–atom empirical dispersion (D) is modified by B97 exchange and correlation functionals. To calculate the structural parameters and vibrational frequencies for the large molecular systems including transition metals, M06-L functional [37], a local meta-GGA approximation, have been commonly used [38]. It is stated that some of the DFT methods are frequently used in the literature, that is, their popularity does not mean that the method gives more successful results in structural, spectral, optical and other molecular properties [39–41]. In this case, it is inevitable that the choice of DFT methods in investigating different properties of materials such as structural, vibrational, electronic and nonlinear optical properties depends on their compatibility with experimental results. Calculating the complex structure with the most possible accuracy at the beginning is extremely important in terms of determining the molecular properties to be examined with high accuracy. The structural, spectral and NLO results for the metal complexes including picolinate and its derivatives were widely investigated by using the DFT approaches (HSEh1PBE and B3LYP methods). The HSEh1PBE and B3LYP methods used in our previous studies distorted the coordination structure of the Zn(II) complex synthesized in the present work. Therefore, the pre-works were performed to determine appropriate DFT methods. As a result of these studies, M06-L and ωB97XD methods were selected due to determining the stable structure of the synthesized complex.

The goal of the current study is to synthesize Zn(II) complex of 6-chloropicolinic acid (6-ClpicH) and picolinic acid (picH) and to characterize the detailed spectral, electrical and optical behaviors. The IC$_{50}$ value of Zn(II) complex against α-glucosidase was also determined. The single crystal structure of the Zn(II) complex was depicted by XRD technique and its spectral and electrical and optical properties were examined by using FTIR and UV–Vis spectra. Optical properties in different molar concentrations in ethanol were investigated. Furthermore, DFT methods (M06-L and ωB97XD) were used to determine structural and spectral behaviors as well as first- and second-order hyperpolarizability parameters. By means of the whole experimental and theoretical parameters, the structure–activity relationships (SAR) were presented for the first time. To determine the complex–protein interactions and to evaluate *in vitro* result, molecular docking was also carried out.

2. Experimental and computational details

2.1. The synthesis of the Zn(II) complex {[Zn(6-clpic)(pic)(H$_2$O)$_2$]}

All chemicals are analytical grade commercial products. 2-Picolinic acid (picH), 6-chloropicolinic acid (6-ClpicH) and zinc(II) acetate dihydrate (Zn(OAc)$_2$·2H$_2$O)) purchased from Sigma-Aldrich were used.

The single crystal X-Ray diffraction (XRD) technique [42–44], FT-IR, NMR and UV–Vis spectrophotometers used for the structural characterizations of Zn(II) complex are presented in the Supplementary Material.

According to the Scheme 1, the synthesis of the Zn(II) complex is fulfilled. The zinc(II) acetate dihydrate (1 mmol) was dissolved in 15 mL of ethanol/water mixture (2:1). The picH (1 mmol) and 6-ClpicH (1 mmol) were added to this solution. This mixture was stirred at 60 °C for 3 h in the closed vial and then allowed to evaporate at room temperature. After 7 days, the colorless prism-shaped single crystals were collected. Synthetic yield: 82.8%. picH: ^{1}H NMR (DMSO d_6, 300 MHz) δ/ppm: 7.56–7.61 (1H, m, Ar-H), 7.92–7.98 (1H, m, Ar-H), 8.01–8.05 (1H, dt, J_1 = 1.1 Hz and J_2 = 7.8 Hz), 8.67–8.69 (1H, dt, J_1 = 1.0 Hz and J_2 = 3.8 Hz), ^{13}C NMR (DMSO d_6, 75 MHz) δ/ppm: 125.4, 127.8, 138.2, 149.0, 150.1, 166.9. 6-ClpicH: ^{1}H NMR (DMSO d_6, 300 MHz) δ/ppm: 7.71–7.74 (1H, m, Ar-H), 8.00–8.03 (2H, m, Ar-H); ^{13}C NMR (DMSO d_6, 75 MHz) δ/ppm: 124.7, 128.6, 141.8, 149.5, 150.8, 165.5. [Zn(6-Clpic)(pic)(H$_2$O)$_2$]:
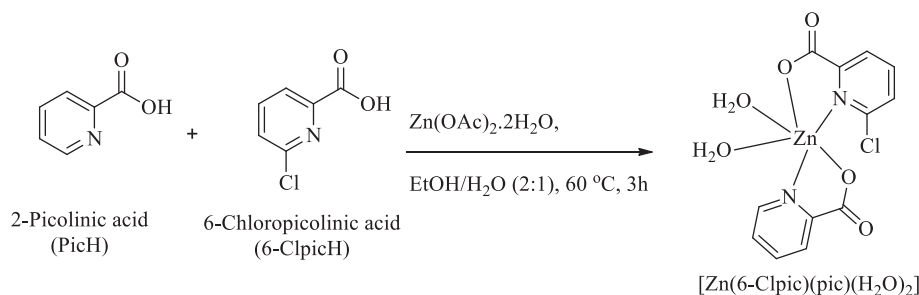
Scheme 1. The synthesis of the Zn(II) complex.

^{1}H NMR (DMSO d_6, 300 MHz) δ/ppm: 3.41 (2x2H, br, H$_2$O), 7.65–7.68 (2H, m, Ar-H), 8.04–8.18 (4H, m, Ar-H), 8.40–8.48 (1H, m, Ar-H); ^{13}C NMR (DMSO d_6, 75 MHz) δ/ppm: 123.5, 124.3, 127.4, 127.8, 141.1, 143.0, 147.0, 148.9, 151.1, 153.1, 165.6, 166.0. The ^{1}H and ^{13}C NMR spectra of the Zn(II) complex are given in Fig. S1 and S2.

2.2. α-Glucosidase inhibition assay

The inhibitory activity of the synthesized Zn(II) complex against α-glucosidase was evaluated by modified Sun's protocol [17–21,45]. By using *p*-nitrophenyl-α-D-glucopyranoside (pNGP, Sigma, N1377) as the substrate, the α-glucosidase from Saccharomyces cerevisiae (Sigma, G5003) was determined as the target protein. The complex and genistein were dissolved in DMSO. The enzyme and the substrate were dissolved in potassium phosphate buffer (0.05 M, pH 6.8). The enzymatic reaction mixture composed of α-glucosidase (0.02 U, 20 μL), substrate (1.25 mM, 30 μL), complex (10 μL) and potassium phosphate buffer (140 μL) was incubated at 37 °C for 30 min. After the incubation, the absorbance of yellow colour produced due to the formation of p-nitrophenol was measured using Synergy H1 (BioTek, USA) 96-well microplate reader at 405 nm. All experiments were performed in triplicates. The inhibitory activity for the Zn complex against α-glucosidase was calculated by using eq. (1):

$$Glucosidase\ inhibition\ =\ [(A_c - A_s)/A_c]x100 \tag{1}$$

In eq. (1), A$_s$ and A$_c$ are the absorbance of sample and control, respectively. Graphpad Software was used for computing IC$_{50}$.

2.3. Computational details

The structural, vibrational, electronic and optical properties of the synthesized complex were investigated by the GAUSSIAN 16, Revision C.01 [46] and GaussView 6 [47] program. DFT/ M06-L and ωB97XD methods [48–50] with 6-311++G(d,p) [51] basis set for H, C, N, O, Cl atoms, and LanL2DZ basis set [52] for Zn atom were applied to calculate the structural geometric parameters and vibrational frequencies of the Zn(II) complex. VEDA program [53,54] including the calculations of potential energy distribution (PED) analysis was used for the assignments of vibrational modes of the Zn(II) complex. Furthermore, the time dependent DFT/ M06-L and ωB97XD (TD–DFT/ M06-L and ωB97XD) levels [55] with conductor–like polarizable continuum model (CPCM) [56] in ethanol and gas phase were used to compute the electronic absorption wavelengths, oscillator strengths (*f*) and transition dipole moments of the Zn(II) complex. The significant contributions came from frontier molecular orbitals (FMOs) in electronic transitions were determined with the help of SWizard [57] program. To depict coordination environment around the Zn(II) center and hydrogen bonding interactions, the natural bond orbital (NBO) [58] calculations were carried out.

For each donor (i) and acceptor (j), the stability energy $E^{(2)}$ including ε_i and ε_j (diagonal elements), $F(i,j)^2$ (the off-diagonal NBO Fock matrix elements) and q_i (the donor orbital occupancy) was calculated by using eq. (2) [10,27,59,60],

$$E^{(2)} = \Delta E_{ij} = q_i \frac{F(i,j)^2}{\varepsilon_i - \varepsilon_j} \tag{2}$$

To detect microscopic linear and nonlinear optical behaviors of the Zn(II) complex in ethanol and gas phase, the electric dipole moment (μ), refractive index (*n*), linear optical parameters ($\bar{\alpha}$, $\Delta\alpha$ and $\chi^{(1)}$), second- and third- order nonlinear optical parameters (β, γ and $\chi^{(3)}$) were calculated at the same levels by using equations below.

The mean and anisotropy of polarizability ($\bar{\alpha}$ and $\Delta\alpha$) parameters were obtained by using eq. (3) and (4) [61–65],

$$\bar{\alpha} = \frac{(a_{xx} + a_{yy} + a_{zz})}{3} \tag{3}$$

$$\Delta a = \left\{ \frac{1}{2} \left[\left(a_{xx} - a_{yy} \right)^2 + \left(a_{yy} - a_{zz} \right)^2 + \left(a_{zz} - a_{xx} \right)^2 \right] \right\}^{1/2} \tag{4}$$

where the Cartesian components of $\bar{\alpha}$ and $\Delta\alpha$ are a_{xx}, a_{yy}, a_{zz}.1 atomic unit (a.u.) of $\bar{\alpha}$ is converted to 0.1482×10^{-24} electrostatic unit (esu).

The theoretical refractive index (*n*) values based on mean polarizability ($\bar{\alpha}$) values in the gas phase and ethanol were obtained by using the Lorentz-Lorenz eq. (5) [10,66],

$$(n^2 - 1)/(n^2 + 2) = D/V \tag{5}$$

where *n* (the refractive index) includes *V* called as the molar volume (cm^3) and D a multiplier depending on Avogadro's number (N_A). *n* is directly calculated as dimensionless from eq. (5) based on $\bar{\alpha}$, *V* and D by using the unit of $\times 10^{-24}$ cm^3, cm^3 and a multiplier of 2.523564179 $\times 10^{24}$.

Based on the Lorentz approximation for the local field, the linear susceptibility ($\chi^{(1)}$) for the Zn(II) complex was calculated by using eq. (6) [10,66],

$$x^{(1)} = \text{N}f\,\bar{\alpha} \tag{6}$$

where f (f = $(n^2 + 3)/3$) is the local field correction factor with respect to Lorentz expression, N is the number of molecules per unit cm^3, mean polarizability ($\bar{\alpha}$) is calculated from eq. (3).

Without using the experimental technique, the third-order nonlinear optical susceptibility ($\chi^{(3)}$) parameter associated with the γ parameter for the Zn(II) complex was found by using the eq. (7) [10,66],

$$c^{(3)} = Nf^4\gamma \tag{7}$$

where N and f is explained above. The second-order hyperpolarizability (γ) parameter was calculated by using eq. (9).

The first- and second-order hyperpolarizability (β and γ) parameters were calculated by using eq. (8) and (9) [61–65],

$$\beta = (\beta_x^2 + \beta_y^2 + \beta_z^2)^{1/2} \tag{8}$$

$$< \gamma > = \frac{1}{5}\left[\gamma_{xxxx} + \gamma_{yyyy} + \gamma_{zzzz} + 2\left(\gamma_{xxyy} + \gamma_{xxzz} + \gamma_{yyzz}\right)\right] \tag{9}$$

where the Cartesian components of β is $\beta_x = \beta_{xxx} + \beta_{xyy} + \beta_{xzz}$,$\beta_y = \beta_{yyy} + \beta_{yxx} + \beta_{yzz}$, $\beta_z = \beta_{zzz} + \beta_{zyy} + \beta_{zxx}$. 1 a.u. is converted to 8.6393×10^{-33} esu for β.

By considering frontier molecular orbital (FMO) energies obtained at the same levels, the molecular parameters (η: Chemical hardness, χ: Electronegativity defined as the negative of chemical potential (μ), S: Chemical softness and ω: Electrophilicity index, φ: Nucleophilicity index) defined as global chemical reactivity descriptors were computed by using eq. (10)-(14) [10,14,67,68].

$$\eta = \frac{(E_{LUMO} - E_{HOMO})}{2} \tag{10}$$

$$\chi = -\frac{(E_{HOMO} + E_{HOMO})}{2} \tag{11}$$

$$S = \frac{1}{\eta} \tag{12}$$

$$\omega = \frac{\chi^2}{2\eta} \tag{13}$$

$$\varphi = \frac{1}{\omega} \tag{14}$$

2.4. Docking procedure

iGEMDOCK program [69] was applied to examine protein–ligand interactions between the synthesized Zn(II) complex used as rigid and target protein (the template structure *S. cerevisiae* isomaltase (PDBID: 3A4A)). The detailed procedure is given in Supplementary Material.

3. Results and discussion

3.1. Structural characterizations

Crystal data and refinement parameters of [Zn(6-Clpic)(pic)(H$_2$O)$_2$] were defined by X-ray diffraction technique (see Table 1). The photograph of single crystal, crystal and theoretical optimized structures of the Zn(II) complex are given in Fig. 1. Fig. 1 demonstrates the coordination geometry of the Zn(II) complex with distorted octahedral geometry. The complex is comprised of the central Zn(II) ion coordinated by one 6-choloropicolinate (6-Clpic), one picolinate (pic) and two water ligands. The theoretical optimization calculations were performed by considering initial parameters of XRD geometry. The experimental and theoretical bond lengths, bond and dihedral angles of the Zn(II) complex are comparatively presented in Table 2. According to the previous works containing Zn(II) complex with picolinate ligands [1,13], it could be said that there is good conformity in the structural parameters around the central metal ions for the Zn(II) complex in this study. In spite of the same metal ion and coordination geometry, the positions of two water ligands are different from each other due to the 6-chloropicolinate ligand having the electronegative chlorine atom in the 6-position.

Table 1
Crystal data and structure refinement parameters for the Zn(II) complex.

|	Zn(II) complex
CCDC Number	2,039,569
Chemical formula	C$_{12}$H$_{11}$ClN$_2$O$_6$Zn
Formula weight	380.05
Crystal color	Colorless
Crystal system	Monoclinic
Space group	$P2_1/n$
Temperature (K)	296
Radiation type	Mo Kα
Wavelength (Å)	0.71073
Crystal size (mm)	0.68 × 0.47 × 0.34
h, k, l	−14 → 14, −10 → 10, −19 → 19
a(Å)	11.5464 (10)
b (Å)	8.8243 (5)
c (Å)	15.7180 (13)
α (°)	90°
β (°)	110.785(6)°
γ (°)	90°
V (Å^3)	1497.3(2)
Z	4
F(000)	768
Density (g cm^{-3})	1.686
μ (mm^{-1})	1.85
θ range (°)	1.9–32.9°
Measured refls.	10,342
Independent refls.	2936
R$_{int}$	0.057
S	1.10
R1/wR2	0.063/0.198
max/min (eÅ^{-3})	0.54/ −1.42

The experimental bond distances of Zn1-N1/O2 (pic) and Zn-N2/O3 (6-Clpic) which allow the formation of a five-membered chelate rings for the complex were observed at 2.127(4)/2.083(4) and 2.288(5)/2.053(3) Å. These theoretical bond lengths at the DFT/M06-L and ωB97XD levels were obtained at the range of 2.090–2.013 Å and 2.209–1.993 Å, respectively. These experimental and theoretical bond distances were obtained longer than those found in the previous studies [1,13]. It can be stated that this is due to the steric and negative inductive effects of the chlorine atom in the 6-choloropicolinate ligand. Based on bond lengths, it can be said that the coordination ability and bond strength of picolinate ligand are better than that of 6-chloropicalinate ligand. In five-membered chelate rings, the experimental and theoretical (M06-L level) bond angles of O2-Zn1-N1 and O3-Zn1-N2 were determined at 78.64(14)/75.26(16)^o and 81.64/78.13 (see Table 2). These angles are coherent with those of [Zn(pic)$_2$(H$_2$O)$_2$]·2H$_2$O reported previously [13].

The O-Zn-O/O-Zn-N/N-Zn-N bond angles defining distorted octahedral geometry for [Zn(6-Clpic)(pic)(H$_2$O)$_2$] were observed at the range from 75.26(16) to 172.58(15), as can be seen in Table 2. The two water ligands of [Zn(6-Clpic)(pic)(H$_2$O)$_2$] complex are located in the equatorial position while those of [Zn(pic)$_2$(H$_2$O)$_2$]·2H$_2$O reported previously [13] are located in the axial position. This position for [Zn(6-Clpic)(pic)(H$_2$O)$_2$] complex is originated from 6-Clpic ligand having high electron density and steric effect due to having the electronegative chlorine atom in the 6-position. In general, it can be said that there is a good consistency between the experimental and theoretical geometric parameters.

The hyperconjugative interaction energies (E$^{(2)}$) from natural bond orbital (NBO) calculations by using the second-order perturbation approach [59,60] were obtained at DFT/M06-L and ωB97XD methods and 6–31++G(d,p)/LanL2DZ basis sets. In addition, the E$^{(2)}$ values defined as the stabilization energy indicate the coordination environment of metal ions in complex structures and their conjugative interactions as well as the strength of the interactions between bonds. The E$^{(2)}$ values obtained at the range from 4.43

(a)
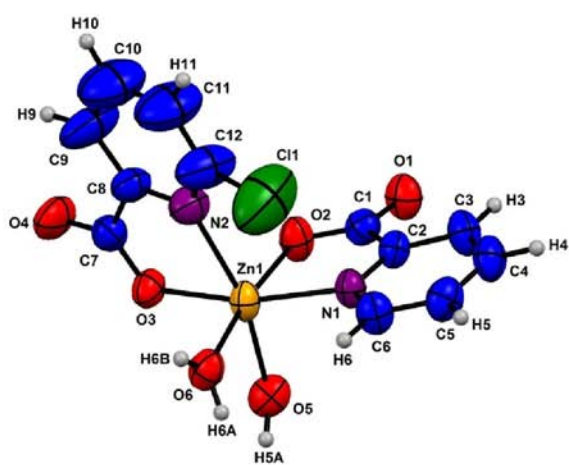
(b)
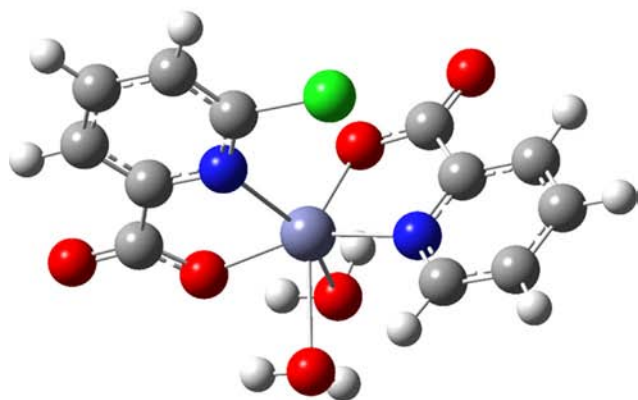
(c)

Fig. 1. (a) Photograph of [Zn(6-Clpic)(pic)(H₂O)₂] single crystal. **(b)** The crystal structure of [Zn(6-Clpic)(pic)(H₂O)₂] with the atomic numbering scheme. The thermal ellipsoids are drawn at the 50% probability level at 296 K. **(c)** The optimized complex molecular structure of [Zn(6-Clpic)(pic)(H₂O)₂] obtained by M06-L level in the gas phase.

Table 2
The experimental and theoretical geometrical parameters of the Zn(II) complex.

Parameters	XRD	M06-L	ωB97XD
Bond lengths (Å)			
Zn1—O6	2.044 (4)	2.397	2.461
Zn1—O3	2.053 (3)	2.033	2.001
Zn1—O2	2.083 (4)	2.013	1.993
Zn1—O5	2.103 (4)	2.388	2.435
Zn1—N1	2.127 (4)	2.090	2.067
Zn1—N2	2.288 (5)	2.199	2.209
O1—C1	1.248 (6)	1.222	1.215
O2—C1	1.249 (6)	1.288	1.282
O4—C7	1.230 (7)	1.219	1.212
O3—C7	1.264 (6)	1.292	1.286
Cl1—C12	1.695 (8)	1.736	1.738
C7—C8	1.510 (8)	1.519	1.530
C1—C2	1.509 (7)	1.527	1.537
N2—C8	1.331 (7)	1.349	1.343
N1—C2	1.337 (7)	1.344	1.338
Bond angles (°)			
O6—Zn1—O3	96.53 (16)	74.39	75.12
O6—Zn1—O2	172.58 (15)	146.8	147.6
O3—Zn1—O2	89.42 (15)	117.9	116.2
O6—Zn1—O5	85.45 (16)	74.34	72.62
O3—Zn1—O5	91.50 (16)	74.18	73.65
O2—Zn1—O5	89.97 (16)	79.72	81.53
O6—Zn1—N1	95.99 (16)	83.37	83.14
O3—Zn1—N1	165.96 (16)	157.7	158.3
O2—Zn1—N1	78.64 (15)	81.64	82.36
O5—Zn1—N1	95.82 (17)	101.1	99.78
O6—Zn1—N2	90.08 (17)	112.8	110.1
O3—Zn1—N2	75.26 (16)	78.13	78.71
O2—Zn1—N2	95.75 (18)	100.1	102.0
O5—Zn1—N2	165.47 (19)	148.2	150.5
N1—Zn1—N2	98.40 (17)	110.3	109.7
C7—O3—Zn1	120.6 (3)	119.68	119.8
Zn1—O6—H6A	126.5	95.42	92.93
Zn1—O6—H6B	127.3	86.60	88.31
Zn1—O5—H5A	127.3	92.88	96.33
Zn1—O5—H5B	125.7	88.73	87.25
C1—O2—Zn1	115.8 (3)	116.0	116.0
C6—N1—Zn1	128.4 (4)	130.0	129.8
C2—N1—Zn1	112.0 (3)	110.1	110.0
C12—N2—Zn1	132.7 (5)	131.1	131.9
C8—N2—Zn1	110.3 (4)	110.2	109.1
Dihedral angles (°)			
Zn1—N1—C2—C3	178.2 (4)	176.6	176.5
Zn1—N1—C2—C1	−4.0 (5)	−3.58	−3.56
Zn1—O3—C7—O4	173.0 (5)	177.8	175.3
Zn1—O3—C7—C8	−9.9 (6)	−2.73	−5.60
Zn1—N2—C8—C9	−175.8 (7)	−172.8	−172.1
Zn1—N2—C8—C7	8.1 (6)	6.98	7.98
Zn1—N1—C6—C5	−178.6 (4)	−175.4	−175.5
Zn1—N2—C12—C11	172.4 (8)	170.5	169.7
Zn1—N2—C12—Cl1	−19.0 (13)	−9.28	−10.5

water ligands were found to be range from 17.85 to 43.06 and from 9.73 to 37.66 kcal/mol (M06-L level), respectively (Table S1). The coordination geometry of the crystal structure for Zn(II) complex defined by the XRD technique was supported by NBO results. The corresponding interactions of the previously reported Zn(II) complexes of pic and 6-methylpicolinate (6-Mepic) ligands were obtained at the range of 13.53 and 47.83 (B3LYP/6–311++G(d,p)/LanL2DZ level) [13], 29.51 and 36.61 kcal/mol (HSEh1PBE/6–311++G(d,p)/LanL2DZ level) [21]. All these results show the occurrence of n → n* interactions for the Zn(II) complex.

Furthermore, the $E^{(2)}$ values of the LP(2)O1 → σ*(C1–C2) and LP(2)O4 → σ*(C7–C8) interactions belonging to the 6-Clpic and pic ligands were appeared at the values of 18.80 and 18.68 kcal/mol (M06-L level) 26.49 and 26.28 (ωB97XD level), as can be seen in Table S1. The electronic configuration of Zn(II) ion was computed as [core]4s$^{(0.31)}$3d$^{(9.98)}$4p$^{(0.41)}$4d$^{(0.01)}$ with 17.9985 core electrons, 10.6966 valence electrons and 0.02201 Rydberg electrons

to 43.06 kcal/mol (M06-L level) and from 5.331 to 53.74 kcal/mol (ωB97XD level) indicate significant interactions of the Zn(II) complex (see Table S1). The n → n* interactions for the Zn(II) complex occur between lone-pair (n) orbitals of *N*, *O* atom and anti-lone-pair (n*) orbitals of Zn(II) ion. The $E^{(2)}$ values indicating the coordination to Zn(II) ion through *N* and *O* atoms of the 6-Clpic, pic and

(ωB97XD level). The natural charge of the Zn(II) ion was calculated at 1.28287e. This charge value which is lower than the free charge ion (2 +) indicates a charge transition from the Zn(II) ion to the picolinate and 6-chloropicolinate ligands. According to the above electronic configuration, it can be said that the picolinate is a non-innocent ligand in this Zn complex because the oxidation state is not clear.

NBO results displayed the stabilization of the complex structure through the bonding and anti-bonding orbitals, interactions between bonds and coordination around metal ions.

It is clear from Table 3 and Fig. S3, the crystal packing structure of Zn(II) complex demonstrates that the O-H⋯O type intermolecular hydrogen bonding interactions emerged at between water ligands and O atoms of carboxylate groups belonging to picolinate/6-chloropicolinate ligands.

3.2. Thermal analysis

Thermogravimetric analysis (TGA, DrTGA and DTA) of the Zn(II) complex was performed by using Shimadzu thermogravimetric analyzer DTG-60H in platinum crucible up to 1000 °C at a heating rate of 10 °C/min in a dry air atmosphere (flow rate of 20 mL/min). As can be seen from Fig. 2, it is clear from the TGA and DrTGA/DTA plots of the Zn (II) complex that the complex is thermally stable up to 69.13 °C and decomposes at higher temperatures in four steps. The first decomposition step occurs at the temperature range from 63.19 °C to 184.99 °C, the complex loses two water molecules (Mass loss: Found 10.033%, Calc. 9.48%). The second and third decomposition steps emerge at the temperature range from 184.99 °C to 470.74 °C, the complex loses chloride and two carbon dioxide molecules (Mass loss: Found 34.45%, Calc. 35.01%). The last decomposition step arises at the temperature range from 470.74 °C to 782.46 °C, the complex loses two pyridine rings (Mass loss: Found 42.326%, Calc. 41.52%). The DTA curve demonstrates a medium and broad endothermic peak at 137.19 °C due to melting and the first decomposition step and a very weak endothermic peak at 330.98 °C related to the second decomposition step. Associated with the third and last decomposition steps, medium and strong broad exothermic peaks appear at 427.62 °C and 638.55 °C, respectively. It was observed that the mass of the complex lost 86.807% and retained 13.193% of its mass between 63.19 °C and 782.46 °C temperatures. It is considered that the remaining product is to be metallic zinc residues. From the results of this analysis, it is clear that the complex is thermally stable up to the melting point and decomposition starts only after the melting point of the material.

3.3. Vibrational analysis

The experimental IR spectra for Zn(II) complex, 6-ClpicH and picH are given in Fig. 3. The theoretical vibrational frequencies of the Zn(II) complex were obtained at DFT//M06-L/ and ωB97XD/6-311++G(d,p)/LanL2DZ levels and scaled by 0.96. VEDA program including the calculations of potential energy distribution (PED) analysis [53,54] was used to assign the vibrational modes of the Zn(II) complex. The selected experimental and theoretical vibrational frequencies are comparatively given in Table 4 and the further vibrational modes are presented in Table S2.

The FT-IR spectra and theoretical vibrational frequencies demonstrate the coordination of pic and 6-Clpic ligands to Zn(II) ion through the carboxylate group (COO⁻), as can be seen in Fig. 3 and Table 4. The υ_{as} and υ_s COO⁻ vibrational bands via FT-IR spectra for the Zn(II) complex were assigned as 1621 and 1375 cm⁻¹. It is well known that the presence of monodentate coordination of COO⁻ group to Zn(II) ion depend on the difference between asymmetric and symmetric stretching frequencies of this group. The experimental/theoretical differences between υ_{as} and υ_s COO⁻ vibrational bands were found to be 246 (experimental)/391 (M06-L level) and 406 cm⁻¹ (ωB97XD level). From Fig. 3 and Table 4, the OH stretching mode displaying the coordination of the water ligands to Zn(II) ion was observed at 3176 cm⁻¹. The corresponding modes were calculated at the range of 3694–3570 cm⁻¹ (M06-L level) and 3755–3645 cm⁻¹ (ωB97XD level), as can be seen in Tables 4 and S2. In reported studies on Zn(II) complexes with picolinate derivatives [13,16,21], depending the electronegative bromine atom and electron-donating methyl group in the 6-position of picolinate ligand, as well as coordination geometry, the OH stretching modes (υ OH) appeared at 3475 and 3343 cm⁻¹ (Zn(II) complex with picolinate), 3355 and 3287 cm⁻¹ (Zn(II) complex with 6-methylpicolinate), and 3224 cm⁻¹ (Zn(II) complex with 6-bromopicolinate (6-Brpic)). The substituent effects in these modes were clearly observed.

The CH stretching mode (υ CH) from FT-IR spectrum belonging to 6-Clpic and pic ligands was assigned as 3062 cm⁻¹. The corresponding theoretical bands of the Zn(II) complex with the range of 99–80% PED contributions were obtained at range from 3099 to 3054 cm⁻¹ and from 3119 to 3073 cm⁻¹ by using M06-L/ and ωB97X/6–311++G(d,p)/LanL2DZ level, respectively (see Tables 4 and S2).

The υ CN and υ CC stretching vibrations of the Zn(II) complexes with pic, 6-Mepic and 6-Brpic ligands were obtained at 1593 and 1244 cm⁻¹ [13], 1593 and 1260 cm⁻¹ [21], 1580 and 1272 cm⁻¹ [16], respectively. In this study, the experimental/theoretical υ CN and υ CC vibrations of the Zn(II) complex were found to be 1561/1570 (M06-L level) and 1155/1141 (M06-L level) cm⁻¹, respectively (Table 4).

The CH in-plane bending (β CH) vibrations have been reported to emerge in the range of 1300–1000 cm⁻¹ [70]. The ring β CH modes of Zn(II) complexes with pic, 6-Mepic and 6-Brpic ligands appeared at 1446–1173 cm⁻¹ range [13], 1466 cm⁻¹ [21], 1580 and 1182 cm⁻¹ range [16], respectively. It is clear from, Tables 4 and S2 while the corresponding vibrational modes for the Zn(II) complex were observed at the range of 1477–1022 cm⁻¹, those of modes with varying PED contributions at the M06-L and ωB97X levels were calculated at the range of 1534–1023 and 1572–1039 cm⁻¹, respectively. The other vibrational modes, such as torsion and out of bending vibrations from IR spectra were assigned in the range 982–643 cm⁻¹ for Zn(II) complex of pic ligands [13], in the range 1014–713 cm⁻¹ for 6-methylpicolinate [21], in the range 1018–404 cm⁻¹ for 6-bromopicolinate [16]. Likewise, theoretical frequencies were calculated at the range 921–642 cm⁻¹ for picolinate [13], in the range 996–709 cm⁻¹ for 6-methylpicolinate [21], in the range 1023–435 cm⁻¹ for 6-bromopicolinate [16]. In present study, these modes were observed at the range from 910 to 431 cm⁻¹ (with FTIR spectra)

Table 3
Hydrogen-bond parameters for the Zn(II) complex (Å and °).

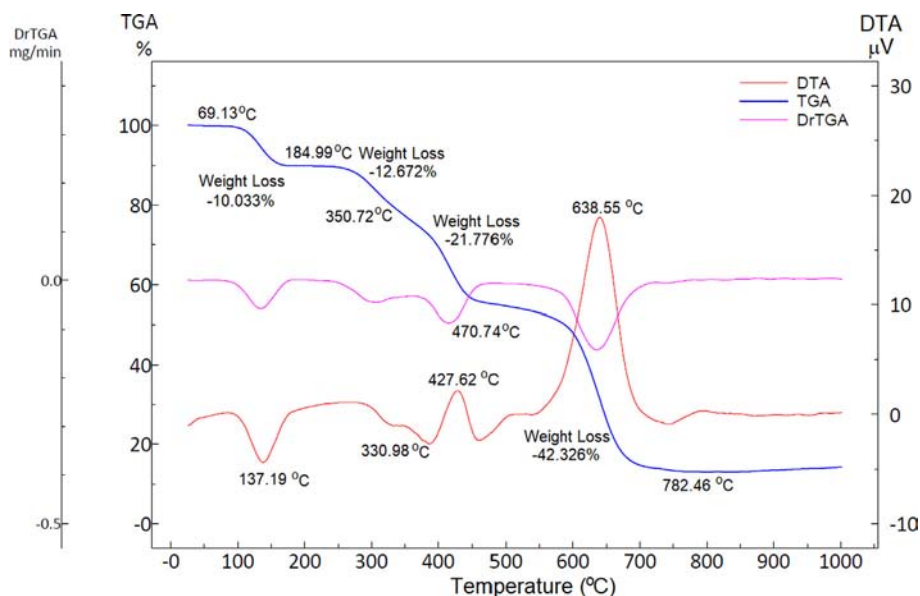| D–H⋯A	D–H	H⋯A	D⋯A	D–H⋯A	Symmetry codes
O5—H5B⋯O1ⁱ	0.85	1.89	2.733 (6)	168	(i) − x, −y + 1, −z + 1
O5—H5A⋯O4ⁱⁱ	0.85	1.86	2.701 (6)	171	(ii) − x + 1/2, y − 1/2, −z + 3/2
O6—H6A⋯O3ⁱⁱ	0.85	1.85	2.671 (5)	163	(ii) − x + 1/2, y − 1/2, −z + 3/2
O6—H6B⋯O1ⁱⁱⁱ	0.85	1.89	2.727 (5)	169	(iii) x + 1/2, −y + 1/2, z + 1/2

Fig.2. TGA, DrTGA and DTA curves of the Zn(II) complex at heating rate of 10 °C/min.

and from 977/997 to 405/408 (with M06-L/ωB97X levels), as can be seen in Tables 4 and S2.

The obtained differences in IR bands for these complexes could be ascribed to the effects of electron–donating (CH$_3$) and –accepting substituents (Cl and Br) located at the 6-position in picolinate derivatives, as well as the strength of coordination bond occurring between ligand and Zn ion. In summary, Tables 4 and S2 display that there is consistency between the experimental and theoretical corresponding vibrational modes of the Zn(II) complex.

3.4. Concentration effects on UV–Vis absorption spectra and optical analysis

The experimental UV–Vis spectra in different molar concentrations in ethanol of the Zn(II) complex were presented in the range

of 200–800 nm (Fig. 4a). By considering this spectra, the optical properties of the Zn(II) complex were investigated. Moreover, TD– M06-L and ωB97X/6–311++G(d,p)/LanL2DZ levels were applied to examine transition dipole moment, oscillator strengths and the electronic absorption wavelengths. Based on these methods, the considerable contributions from molecular orbitals between ligands and metal ion were determined by using SWizard [57] and Chemissian [71] programs. The obtained results are given in Table 5.

Fig. 4a displays the UV–Vis absorption spectra of the Zn(II) complex at 13, 33, 44 and 94 μM concentrations in ethanol. While the absorption intensities changed at these concentrations, the electronic absorption wavelengths were observed at the same position. Three maximum absorption bands for the Zn(II) complex appeared at 365 and 267 and 215 nm (see Fig. 4a). Theoretical absorption
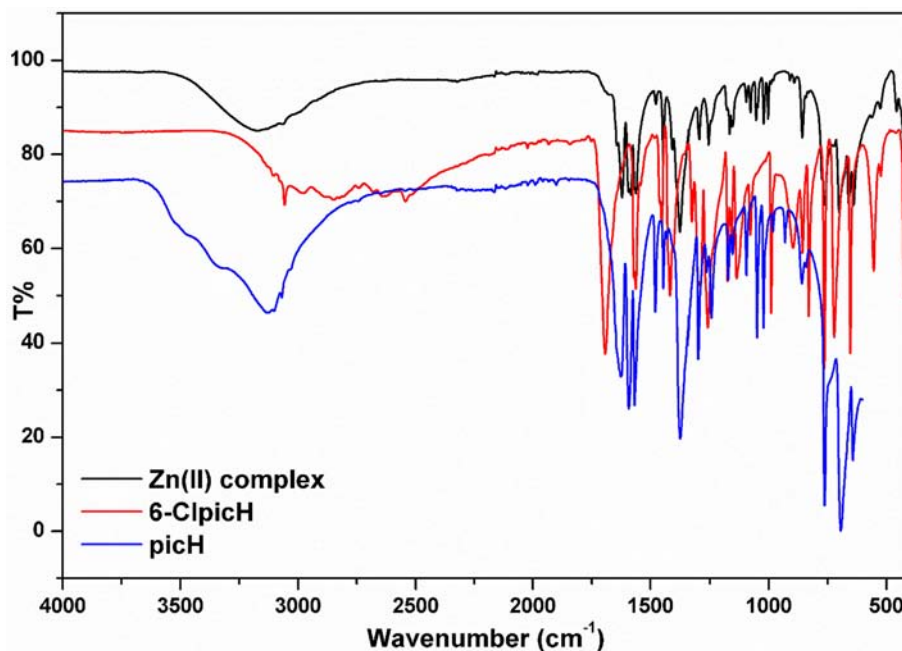

Fig. 3. The FT-IR spectra of the Zn(II) complex, 6-ClpicH and picH at the range of a 4000–400 cm^{-1}.

Table 4
The selected experimental and theoretical characteristic vibrational frequencies for the Zn(II) complex.

Assignments via PED% (with M06-L)	FT–IR	M06-L			ωB97XD		
Complex **1**		Scaled freq[a]	I_{IR}^b	I_{Ra}^c	Scaled freq[a]	I_{IR}^b	I_{Ra}^c
υ$_{as}$ OH 100%		3694	132.0064	19.9908	3755	138.1330	17.0011
υ$_s$ OH 97%	3176	3570	61.9785	46.7660	3645	73.5816	64.5526
υ CH 93%	3062	3067	2.6170	96.1997	3091	0.1715	54.9358
υ OC 92%		1697	209.8295	57.9414	1737	296.3536	38.5725
υ OC 81%	1621	1687	762.3338	40.3194	1723	823.8567	23.4740
β HOH 84%	1593	1605	77.4447	1.2490	1609	48.5234	0.7959
υ CC 63%	1584	1584	46.1428	22.6546	1603	74.4266	16.3529
υ NC 11%+ υ CC 36%+β CCC 11%	1561	1570	62.1322	22.5679	1585	106.6818	1.4589
υ CC 58%+ β HCC 12%	1477	1534	72.2997	19.0586	1572	92.0608	20.5570
υ CC 15%+ β HCC 48%	1407	1407	8.6465	3.5023	1390	26.2132	2.1176
υ OC 32%	1375	1306	144.4502	47.8050	1331	258.0968	46.0661
υ OC 22%+ υ NC 14%	1295	1301	160.5737	12.1691	1320	349.9025	7.9656
υ OC 21%+ υ NC 29%	1256	1264	206.3546	19.9858	1253	40.8814	6.0751
υ OC 15%+ β HCC 24%	1166	1149	16.6250	9.5193	1174	11.3890	1.4674
υ OC 15%+ υ CC 36%+ β HCC 16%	1155	1141	18.6747	9.0759	1155	16.0800	6.5357
υ CC 10%+ υ ClC 10%+ β HCC 32%+ β CNC 16%	1079	1113	31.1080	7.7563	1127	9.7029	5.1982
υ CC 17%+ β HCC 39%	1053	1065	5.6964	10.7721	1084	8.5855	8.7717
υ CC 32%+ β HCC 53%	1045	1044	17.2265	1.3883	1076	20.3087	2.1039
β CCN 13%+ β HCC 12%+ β CNC 27%+β CCC 19%	1022	1023	21.0575	5.8984	1039	23.2804	6.2279
υ NC 24%+ β CCN 40%+ β CNC 17%	1003	1004	8.7813	38.0027	1016	8.1120	32.5203
υ CC 25%+ β CCC 43%+ β NCC 10%	981	985	15.6409	34.0265	1010	0.1551	0.3322
υ CC 18%+ υ ClC 14%+ β OCC 28%	858	850	11.4095	2.8607	862	19.1338	2.9618
υ ClC 12%+ β OCC 26% + β CCC 13%	700	741	77.1508	1.8940	754	73.6515	1.4435
υ CC 15%+ β CCC 33% + β NCC 12%	660	652	6.1702	9.1768	658	3.7066	5.2077
υ ZnN 10%+ β CCN 11% + β CNC 28%+ β CCC 35%	640	635	9.9096	2.9955	644	22.7837	2.6727
υ CC 25%+ β OCC 15%+ β NCC 12%	456	434	5.7765	1.6989	443	4.8293	2.6730
υ CC 11%+ τ CCNZn 13%	431	430	5.7018	1.9103	441	23.5634	1.4414
υ ClC 39%+ β CNC 11%+ β ClCC 11%	411	407	4.8054	2.7359	415	4.2415	0.0564

υ: Stretching; β: In plane bending; τ: Torsion; γ: Out of plane bending.
[a] Scaled frequency are in unit of cm⁻¹; [b] I_{IR} infrared intent. are in unit of km mol⁻¹; [b] I_{Ra} Raman activity is in unit of Å⁴/amu.
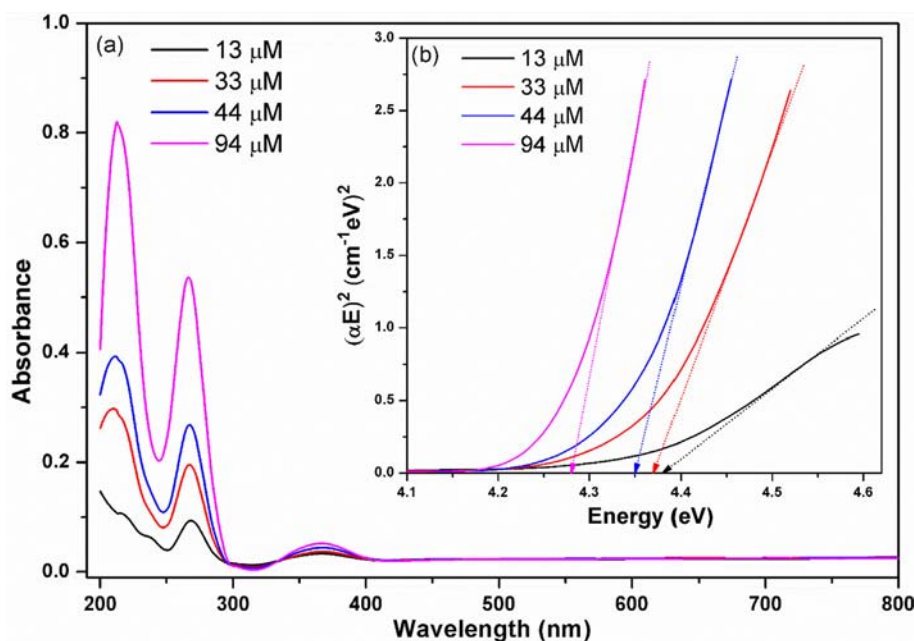
Fig. 4. (a) The UV–vis spectra and **(b)** the plots of $(\alpha E)^2$ vs. E of the Zn(II) complex at 13, 33, 44 and 94 μM concentrations in ethanol.

wavelengths corresponding to these bands in ethanol were obtained at 371.1, 261.2 and 215.4 nm calculated at TD–M06-L/6–311++G(d,p)/LanL2DZ level, respectively. It has been shown that the increasing contribution of metal orbitals to the LUMO of the complex increased the π-acceptor property of the ligand [72]. While the contribution of the Zn orbitals to the HOMO and LUMO of the complex obtained at the TD-M06-L and ωB97X calculations ranges from 1% to 15% (HOMO) and from 1% to 9% (LUMO), the con-

tributions of ligands 6-Clpic and pic to the HOMO/LUMO range from 11% to 72% (HOMO)/from 8% to 59% (LUMO) for 6-Clpic and from 24% to 97% (HOMO)/from 40% to 91% (LUMO) for pic (see Table 5). It can be stated that pic moiety is a much stronger π-acceptor than 6-Clpic in the Zn(II) complex because the LUMO contribution of pic is higher than that of 6-Clpic. The contributions of the ligands pic and 6-Clpic orbitals to the different ten highest filled MOs in the Zn(II) complex range from 27% to 86% and from

Table 5

The experimental and theoretical electronic absorption wavelengths, transition dipole moments and oscillator strength for the Zn(II) complex.

Solvent	Exp. λ (nm)	TD–M06-L/6-311++G(d,p)/LanL2DZ			
		λ (nm)	Osc. strength	μ_{eg} (D)	Major contributions determined via SWizard//Chemissian program 6-Clpic: 6-Chloropicolinate; pic: Picolinate; W: Water ligands; H: HOMO; L: LUMO
Ethanol					
	365	371.1	0.0044	0.587	(100%) H [Zn(1%) + Pic(86%) + 6-Clpic(13%)] → L [(Zn(%1) + Pic(77%) + 6-Clpic(22%)]
	267	261.2	0.0168	0.966	(82%) H-3 [Zn(7%) + Pic(36%) + 6-Clpic(57%)] → L + 2 [Zn(2%) + Pic(50%) + 6-Clpic(48%)]
		259.5	0.0797	2.098	(36%) H-6 [Zn(5%) + Pic(27%) + 6-Clpic(66%) + W(2%)] → L [Zn(%1) + Pic(77%) + 6-Clpic(22%)]
					(17%) H-3 [Zn(7%) + Pic(36%) + 6-Clpic(57%)] → L + 2 [Zn(3%) + Pic(50%) + 6-Clpic(48%)]
	215	215.4	0.0543	1.577	(38%) H-9 [Zn(2%) + Pic(55%) + 6-Clpic(42%)] → L + 1 [Zn(5%) + Pic(85%) + 6-Clpic(9%)]
					(38%) H-7 [Zn(4%) + Pic(82%) + 6-Clpic(14%)] → L + 3 [Zn(6%) + Pic(51%) + 6-Clpic(42%)]
Gas phase					
		364.1	0.0019	0.382	(100%) H-1 [Zn(3%) + Pic(24%) + 6-Clpic(72%)] → L + 1 [Zn(1%) + Pic(91%) + 6-Clpic(8%)]
		268.8	0.0068	0.624	(59%) H-3 [Zn(12%) + Pic(78%) + 6-Clpic(9%)] → L + 3 [Zn(1%) + Pic(79%) + 6-Clpic(20%)]
					(31%) H-2 [Zn(8%) + Pic(61%) + 6-Clpic(30%)] → L + 3 [Zn(1%) + Pic(79%) + 6-Clpic(20%)]
		259.7	0.0559	1.757	(42%) H-6 [Zn(6%) + Pic(34%) + 6-Clpic(58%) + W(2%)] → L [Zn(3%) + Pic(65%) + 6-Clpic(31%)]
					(15%) H-7 [Zn(2%) + Pic(83%) + 6-Clpic(14%)] → L [Zn(3%) + Pic(65%) + 6-Clpic(31%)]
		215.1	0.0020	0.299	(93%) H-1 [Zn(3%) + Pic(24%) + 6-Clpic(72%)] → L + 6 [Pic(40%) + 6-Clpic(59%)]
		TD–ωB97XD/6-311++G(d,p)/LanL2DZ			
Ethanol					
	365				
	267	264.4	0.0002	0.114	(58%) H-1 [Zn(2%) + Pic(45%) + 6-Clpic(53%)] → L [Zn(2%) + Pic(73%) + 6-Clpic(24%)]
					(12%) H [Zn(1%) + Pic(85%) + 6-Clpic(14%)] → L [Zn(2%) + Pic(73%) + 6-Clpic(24%)]
		263.0	0.0003	0.133	(70%) H [Zn(1%) + Pic(85%) + 6-Clpic(14%)] → L + 1 [Zn(9%) + Pic(77%) + 6-Clpic(14%)]
					(7%) H [Zn(1%) + Pic(85%) + 6-Clpic(14%)] → L + 3 [Zn(6%) + Pic(42%) + 6-Clpic(52%)]
		242.9	0.1550	2.830	(65%) H-2 [Zn(3%) + Pic(65%) + 6-Clpic(31%)] → L [Zn(2%) + Pic(73%) + 6-Clpic(24%)]
					(12%) H-1 [Zn(2%) + Pic(45%) + 6-Clpic(53%)] → L [Zn(2%) + Pic(73%) + 6-Clpic(24%)]
	215	214.2	0.0058	0.516	(39%) H [Zn(1%) + Pic(85%) + 6-Clpic(14%)] → L + 3 [Zn(6%) + Pic(42%) + 6-Clpic(52%)]
					(24%) H-10 [Zn(2%) + Pic(47%) + 6-Clpic(47%) + W(2%)] → L + 1 [Zn(9%) + Pic(77%) + 6-Clpic(14%)]
Gas phase					
		289.3	0.0002	0.1032	(77%) H [Zn(1%) + Pic(97%) + 6-Clpic(2%)] → L + 1 [Zn(2%) + Pic(85%) + 6-Clpic(13%)]
					(13%) H [Zn(1%) + Pic(97%) + 6-Clpic(2%)] → L + 3 [Zn(1%) + Pic(52%) + 6-Clpic(47%)]
		283.9	0.0003	0.1287	(78%) H-1 [Zn(4%) + Pic(31%) + 6-Clpic(65%)] → L [Zn(4%) + Pic(65%) + 6-Clpic(31%)]
					(9%) H-1 [Zn(4%) + Pic(31%) + 6-Clpic(65%)] → L + 2 [Zn(2%) + Pic(52%) + 6-Clpic(46%)]
		242.3	0.1115	2.3968	(70%) H-3 [Zn(13%) + Pic(39%) + 6-Clpic(42%)] → L [Zn(4%) + Pic(65%) + 6-Clpic(31%)]
					(9%) H-10 [Zn(3%) + Pic(37%) + 6-Clpic(59%)] → L + 2 [Zn(2%) + Pic(52%) + 6-Clpic(46%)]
		219.1	0.0222	1.0175	(58%) H-2 [Zn(15%) + Pic(49%) + 6-Clpic(36%)] → L + 1 [Zn(2%) + Pic(85%) + 6-Clpic(13%)]
					(25%) H-5 [Zn(2%) + Pic(86%) + 6-Clpic(11%)] → L + 1 [Zn(2%) + Pic(85%) + 6-Clpic(13%)]

13% to 66% (TD-M06-L level in ethanol), respectively. These contributions obtained at TD-M06-L and TD-ωB97X in the gas phase show similar variations. Therefore, the degree of covalency in the Zn-pic bonding is much higher than in the bonding between Zn and 6-Clpic/water ligands. Fig. 5 displays the most active FMOs in electronic transition of the Zn(II) complex obtained by M06-L level in ethanol. The HOMO of the Zn(II) complex is mainly centered on the Zn and pic ligand with minor contributions of the two oxygen atoms of 6-Clpic ligand. The main lobes of the LUMO are localized on the 6-Clpic ligand. According to the TD-M06-L calculation in ethanol, the lowest energy transition (with the low oscillator strengths (*f*) and transition dipole moments (μ_{eg})) correspond to the metal-to-ligand charge transfer (MLCT) transition was determined as the H → L(100%), as can be seen in Table 5. In this transition, the contributions of the ligands pic and 6-Clpic orbitals to the HOMO and LUMO range from 86% to 77% (for pic) and from 13% to 22% (for 6-Clpic), respectively. The gas phase TD-M06-L calculation demonstrates MLCT transition with the contribution of H-1 → L + 1(100%) between Zn and pic/6-Clpic ligands formed by different percentage contribution values. However, these lowest energy transitions obtained at TD-M06-L level in the ethanol and gas phase are not observed at the TD-ωB97X level. The bands at 261.2, 259.5 and 215.4 nm obtained at TD-M06-L level in the ethanol (*f* = 0.0168, 0.0797, 0.0543 and μ_{eg} = 0.966 D, 2.098 D and 1.577 D) display the electronic transitions formed by H-3 → L + 2(82%), H-6 → L(36%) and H-9 → L + 1(38%) excitations. These transitions with these high oscillator strengths and transition dipole moments exhibit metal–ligand/ligand–metal and ligand–ligand charge

transfer stemmed from Zn, ligands pic and 6-Clpic by different percentage contribution.

The coordinations around Zn(II) ion of the [Zn(6-Clpic)(pic) $(H_2O)_2$] and [Zn(6-Brpic)$_2$(H$_2$O)$_2$]·H$_2$O [16] complexes were similarly defined as a distorted octahedral geometry, but the coordination of the [Zn(6-Mepic)$_2$(H$_2$O)]·2H$_2$O [21] was described as a distorted trigonal bipyramid. Regardless of the coordination geometry of these complexes, two absorption peaks were obtained at close values with slight differences depending on the coordination ligands. These absorption values attributed to n → π* and π → π* transitions were observed at 265 and 215 nm for [Zn(6-Clpic)(pic) $(H_2O)_2$], 277.33 and 228.01 nm for [Zn(6-Brpic)$_2$(H$_2$O)$_2$]·H$_2$O, 272 and 217 nm for [Zn(6-Mepic)$_2$(H$_2$O)]·2H$_2$O due to the 6-Clpic/6-Brpic/6-Mepic ligands having the electronegative chlorine and bromine atoms and electron electron–donating methyl group in the 6-position.

Optical properties were investigated by using the transmittance and the reflectance spectra of the Zn(II) complex at 13, 33, 44 and 94 μM concentrations in ethanol (Fig. S4). By considering the Tauc and Menth's model, the type of optical transition and the energy band gap is obtained from the following eq. (15) [73–76]

$$(\alpha h\nu) = A(h\nu - E_g)^m \tag{15}$$

In eq. (15), the absorption coefficient (α) including the transmittance (T) and the length of the cuvette (d) taken as 1 cm was found by $\alpha = -2.303 \log T/d$ [74,77]. The $h\nu$ is the photon energy, E_g is the
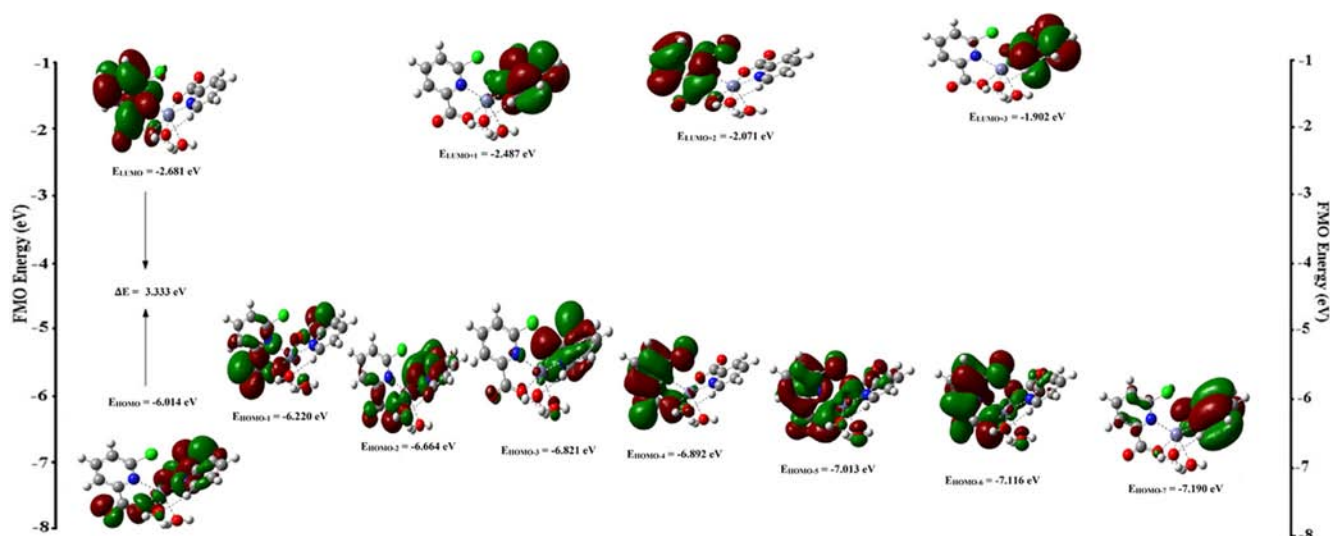
Fig. 5. The most active occupied and unoccupied molecular orbitals in electronic transition of the Zn(II) complex obtained by M06-L level in ethanol.

band gap energy and *A* is a constant. The exponent *m* for allowed direct and indirect transition is taken as 1/2 and 2, respectively.

By regarding the curve of dT/dλ vs λ, the band edge energy of the Zn(II) complex was obtained. From Fig. S5, the corresponding E_{g-abs} energy of maximum peaks in different molar concentrations emerged at 281.7, 281.2, 280.7 and 280.1 nm was found to be 4.43, 4.42, 4.41 and 4.40 eV, respectively (see Table 6). Consequently, these values are consistent with direct transition (*m* = 1/2) for the Zn(II) complex. For this reason, by extrapolating the linear portion of the plot relating $(\alpha h\nu)^2$ against $(h\nu)$ to $(\alpha h\nu)^2 = 0$ in Fig. 4b, the optical band gap energy values in different molar concentrations were found to be 4.38, 4.37, 4.35 and 4.28 eV (see Table 6). Despite the difference between molar concentrations, the band gap energies of the Zn(II) complex were obtained at the results close to each other.

Furthermore, the absorption coefficient α described by the Urbach formula [74,78] exponentially shows the dependence on photon energy in the region of $h\nu \leq E_g$

$$\alpha(h\nu) = \alpha_0 \exp\left(\frac{h\nu}{E_u}\right) \qquad (16)$$

In eq. (16), α_0 is constant and E_u is the Urbach energy interpreted as the width of the localized states. Based on Fig. 6, Urbach energies obtained at the range of 190 and 102 meV for the Zn(II) complex were computed from the inverse of the slope of the linear portion of the curves $ln\alpha$ vs. $h\nu$. The E_u value for [Zn(6-Brpic)$_2$(H$_2$O)$_2$]·H$_2$O complex was found to be 56.5 meV regardless of molar concentrations. These results obtained at the low Urbach energy display that it could be minimal defect in the structure of Zn(II) complex.

The calculations of frontier molecular orbital (FMO) referred to the HOMO and LUMO energies allowing the determination of molecular hardness, softness, electrophilic and nucleophilic indexes play a key role on chemical reactivity and biological activ-

ity of molecular systems. The experimental band gap (E_g) value of the Zn(II) complex at different molar concentrations was obtained at an average of 4.35 eV (see Fig. 4b) and theoretical energy gap values in ethanol and gas phase were calculated as 3.333 and 2.825 eV from FMO energies with M06-L level. According to the previous studies on Zn(II) and Co(II) complexes of pyridine derivatives [79,80]. The band gaps for the Zn(II) complexes of pic, 6-Mepic and 6-Brpic ligands were reported at 4.8534 [13], 4.22 [21] and 4.67 eV [16], respectively. These results display the strengths of electron–accepting (Cl and Br) and electron–donating (methyl group) located at the 6-position.

The values of χ, η, S, ω and φ parameters called as electronegativity, chemical hardness, chemical softness, electrophilicity and nucleophilicity indexes obtained from FMO energies with M06-L level were obtained at 4.348 eV, 1.667 eV, 0.600 eV^{-1}, 5.670 eV and 0.176 eV^{-1}, respectively. In comparison of the χ, η, and S results for the Zn(II) complexes of pic [13], 6-Mepic [21] and 6-Brpic [16], it is clear that the results show consistency in measurability. The electrophilicity index depending on maximal electron flow between donor and acceptor can be ranked as 4.152 eV ([Zn(pic)$_2$(H$_2$O)$_2$]·2H$_2$O) < 4.463 eV ([Zn(6-Mepic)$_2$(H$_2$O)]·2H$_2$O) < 4.781 eV ([Zn(6-Brpic)$_2$(H$_2$O)$_2$]·H$_2$O) < 5.670 eV ([Zn(6-Clpic)(pic)(H$_2$O)$_2$]). It can be said that the presence of the methyl and halogen substituents in the Zn(II) complexes decreases electrophilic property due to the rising electron density.

The molecular electrostatic potential (MEP) surface analysis [81,82] is a useful method that provides predictions for intermolecular interactions and molecular properties of systems such as drug molecules and their analogues. The MEP surface of the Zn(II) complex obtained at M06-L/6–311++G(d,p)/LanL2DZ level is given in Fig. 7. As seen in Fig. 7, it is observed that the red colored negative regions showing electrophilic reactivity are on the uncoordinated electronegative O atoms belonging to the carboxylate

Table 6
The optical parameters of the Zn(II) complex at 13, 33, 44 and 94 μM concentrations in ethanol.

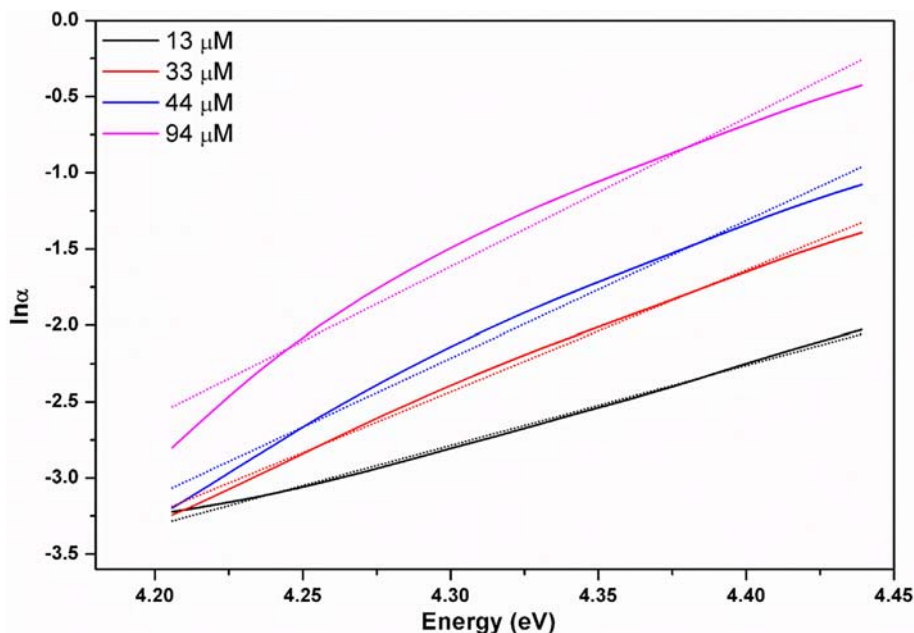| Molar concentration	E_{g-abs} (eV)	E_g (eV)	E_u (meV)	E_o (eV)	E_d (eV)	n_o	f (eV)^2	M_{-1} x(10^{-2})	M_{-3} (eV)$^{-2}$ x(10^{-2})
13 μM	4.43	4.38	190	3.96	1.50	1.173	5.94	38	2.41
33 μM	4.42	4.37	125	3.84	1.34	1.162	5.15	35	2.37
44 μM	4.41	4.35	111	3.70	1.16	1.146	4.30	31	2.29
94 μM	4.40	4.28	102	3.58	0.94	1.124	3.37	26	2.05

Fig. 6. The plots of *lnα* vs. *E* of the Zn(II) complex at 13, 33, 44 and 94 μM concentrations in ethanol.

group of the 6-Clpic and pic ligands, while the blue colored positive regions showing the nucleophilic reactivity are on the C-H bonds of ligands.

3.5. Concentration effects on the refractive index, linear and non-linear optical analysis

The refractive index (n) and extinction coefficient (k) for the Zn (II) complex at 13, 33, 44 and 94 μM concentrations in ethanol were obtained by using the following equations [74–76],

$$n = \frac{1+R}{1-R} + \sqrt{\frac{4R}{(1-R)^2} - k^2} \tag{17}$$

$$k = \frac{\alpha\lambda}{4\pi} \tag{18}$$

In eq. (17) and (18), R, α and λ is the reflectance, absorption coefficient and wavelength, respectively. The refractive index values of the Zn(II) complex at 13, 33, 44 and 94 μM concentrations were obtained at 1.50, 1.54, 1.59, 1.65 at 365 nm, respectively (see Fig. 8a). The extinction coefficient of the complex appears at the minimum peak of 0.22×10^{-6}, 0.24×10^{-6}, 0.29×10^{-6} and 0.34×10^{-6} at 365 nm (see Fig. 8b). It can be concluded that these results with respect to the different concentrations exhibit the same behaves similarly as the concentration increases and decreases.

The dispersion of refractive index (n) was considered in the investigation of optical materials because of a crucial factor in the optical communication and the designing of optical devices. Equation (19) including E_o defined as the oscillator energy in electronic transitions and the dispersion energy E_d defined as a measure of the strength of interband transition is used to calculate the n index below the absorption edge depending on the photon
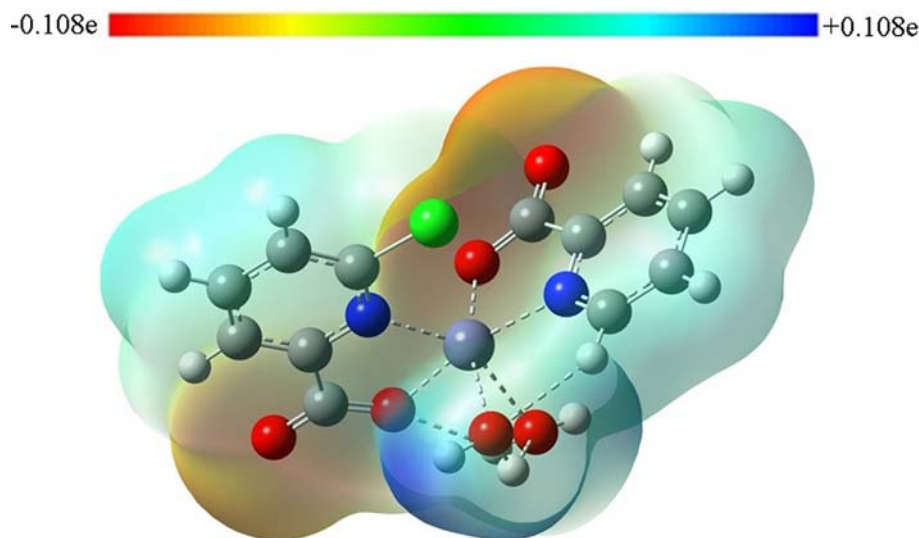

Fig. 7. Molecular electrostatic potential (MEP) surfaces for Zn(II) complex obtained by M06-L level in ethanol.
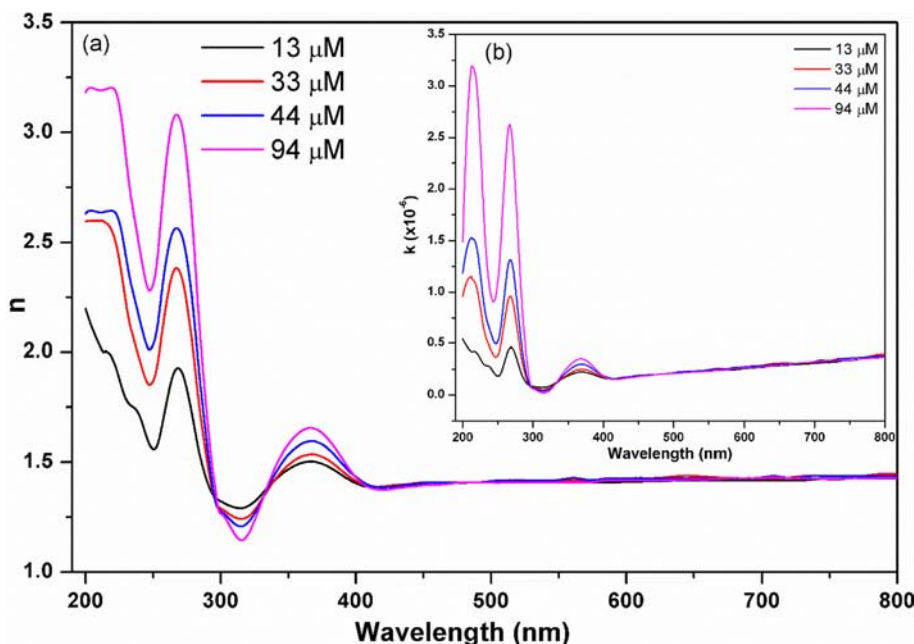
Fig. 8. (a) The refractive index *n* and **(b)** the extinction coefficient *k* vs. *λ* of the Zn(II) complex at 13, 33, 44 and 94 μM concentrations in ethanol.

energy (*hv*) with Wemple-DiDomenico's single oscillator model [74,83,84].

$$\frac{1}{n^2 - 1} = \frac{E_o^2 - (hv)^2}{E_o E_d} \qquad (19)$$

By regarding the slope $(E_o E_d)^{-1}$ and the intercept (E_o/E_d) on the vertical axis by fitting the linear part of the curves, the values of E_o and E_d were determined from Fig. 9. The E_o and E_d values for the Zn(II) complex at 13, 33, 44 and 94 μM concentrations in the ethanol obtained at the range of 3.96–3.58 eV and 1.50–0.94 eV from are bigger than those of the $[Zn(6\text{-Brpic})_2(H_2O)_2]\cdot H_2O$ complex [16]. Besides, the oscillator strength (*f*), M_{-1} and M_{-3} moments associated with E_o and E_d from optical spectra for the Zn(II) complex were calculated by using eq. (20) [15,73,80,81],

$$E_o^2 = \frac{M_{-1}}{M_{-3}} E_d^2 = \frac{M_{-1}^3}{M_{-3}} f = E_d E_o \qquad (20)$$

The M_{-1} and M_{-3} values of the synthesized Zn(II) complex were obtained larger than those of the Zn(II) complex with 6-Brpic ligands (see Table 6).

The investigation of NLO molecular systems to meet the emerging requirements areas, such as optical telecommunications is considerable. In this regard, the select of ligands in coordination complex structures due to the strength and versatility of the metal–ligand bonds in the synthesizing non-centrosymmetric systems in crystal structures have been gaining importance for the synthesis of materials exhibiting the second- and third-order non-linear optical property. NLO materials showing fast reaction times and easy workability is significant for the applications of optoelectronic and photonic technology.

In present work, the linear optical susceptibility ($\chi^{(1)}$) and third-nonlinear optical susceptibility ($\chi^{(3)}$) parameters were examined without Z-scan technique [85,86]. The experimental average refractive index (*n*) was obtained from the graph of the refractive index versus the wavenumber in the mid-IR region (4000–400 cm^{-1}) by using eq. (17), as can be seen in Fig. S6. The *n* of the Zn(II) complex were found to be 1.49 and corresponding theoretical *n* calculated at 1.86/1.52 and 1.75/1.41 in ethanol/gas phase using M06-L and ωB97XD levels, respectively The experi-

mental and theoretical *n* for the Zn(II) complex of the 6-Brpic ligand were obtained at 1.629 and 1.42 [16].

Furthermore, by considering the local-field polarizability model of Clausius– Mossotti, the between molar polarizability (α_p) and refractive index (*n*) in the UV–Vis region (200–800 nm) is given by eq. (21) [87,88].

$$\alpha_p = \frac{3M}{4\pi N_a \rho} \left(\frac{n^2 - 1}{n^2 + 2}\right) \qquad (21)$$

In eq. (21), N_a is the Avogadro number, *M* and ρ are the molecular weight and density, respectively. While the molar polarizability does not change up to about 3 eV, the Zn(II) complex has a molar polarizability of 67.33x 10^{-24} cm^3 versus 5.6 eV photon energy at 94 μM concentrations in ethanol, depending on the change of molar concentrations (see Fig. 10a). As a result, as can be seen from Fig. 10a, the polarizability values also increase with the increase in molar concentration corresponding to the photon energy values of 3.4 and 4.6 eV. The $\chi^{(3)}$ parameter in the UV–Vis region (200–800 nm) depending on refractive index is calculated by using eq. (22) [87,88].

$$\chi^{(3)} = \frac{A}{(4\pi)^4} (n^2 - 1)^4 \qquad (22)$$

In eq. (22), the *A* parameter for all materials is approximately used to 10^{-10} esu regardless of frequency. It could be sated from Fig. 10a,b that there is a coherent between the curves of third-order nonlinear optical susceptibility $\chi^{(3)}$ and molar polarizability α_p. From Fig. 10b, while the $\chi^{(3)}$ values did not change up to about 4.3 eV, the $\chi^{(3)}$ values at 94 μM concentration corresponding to the photon energies of 4.6 and 5.7 eV were observed at 206.6 × 10^{-13} and 294.3 × 10^{-13} esu. It is seen that third-order nonlinear optical susceptibility $\chi^{(3)}$ increases due to the increase in molar concentration.

Theoretical refractive index, linear and nonlinear optical parameters for the Zn(II) complex in the gas phase and ethanol were investigated by using DFT/M06-L and ωB97XD methods with 6–311++G(d,p) basis set. In addition, the experimental and theoretical *n*, $\bar{\alpha}$ and $\chi^{(1)}$ parameters were surveyed. Since the experimental μ, β and γ parameters could be not obtained, these parameters
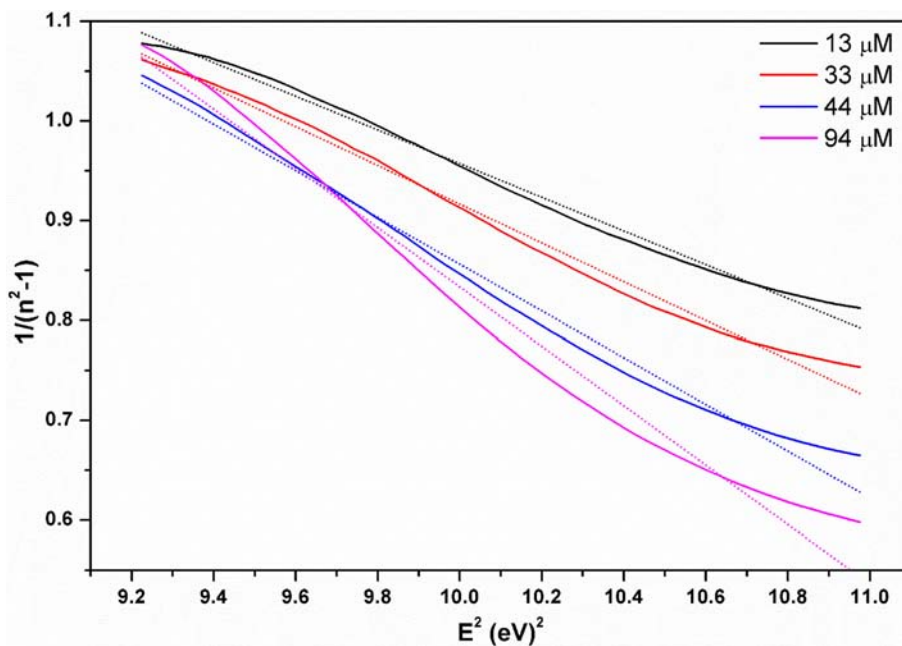
Fig. 9. The plots of *(1/n²-1)* vs. *E²* of the Zn(II) complex at 13, 33, 44 and 94 μM concentrations in ethanol.
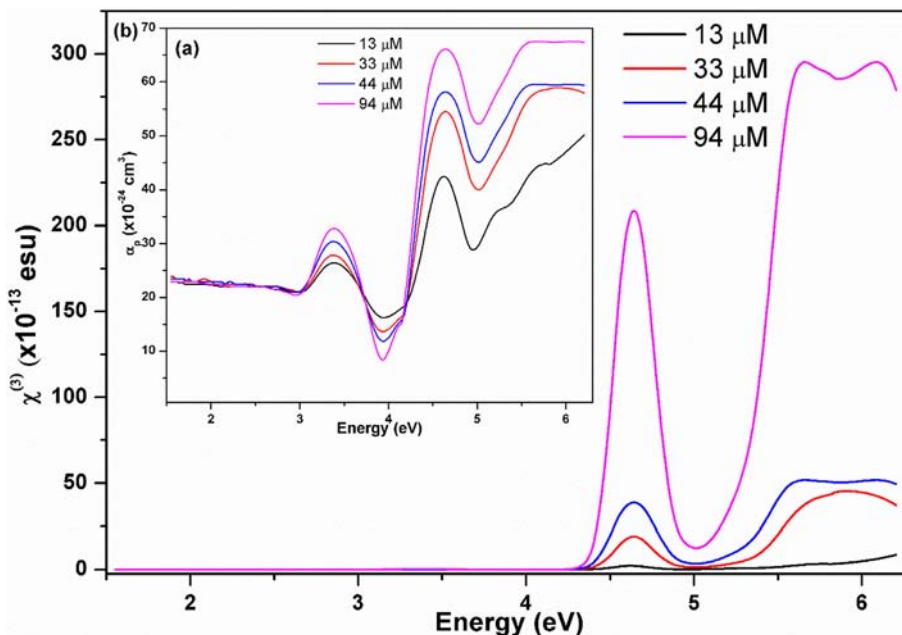

Fig. 10. **(a)** The molar polarizability α_p and **(b)** the third-order nonlinear optical susceptibility $\chi^{(3)}$ of the Zn(II) complex at 13, 33, 44 and 94 μM concentrations in ethanol.

calculated theoretically were compared with the results of p-nitroaniline (pNA) [89] and urea [90] using as prototype materials. The experimental $\bar{\alpha}$, n, $\chi^{(1)}$ and theoretical μ, $\bar{\alpha}$, $\Delta\alpha$, n, $\chi^{(1)}$, β, γ and $\chi^{(3)}$ parameters of the Zn(II) complex are presented in Table 7. The experimental n in mid-IR region of the complex was found to be 1.49 (see Fig. S6) and corresponding theoretical n calculated at 1.86/1.52 and 1.75/1.41 in ethanol/gas phase using M06-L and ωB97XD levels, respectively. The experimental linear optical $\bar{\alpha}$ and $\chi^{(1)}$ parameters for the Zn(II) complex were obtained at 25.83 × 10⁻²⁴ and 12.01 × 10⁻² esu. These parameters for the complex in ethanol were found to be 40.93 × 10⁻²⁴ and 24.45 × 10⁻² esu, 39.52 × 10⁻²⁴ and 21.91 × 10⁻² esu by using M06-L and

ωB97XD levels, respectively (see Table 7). The experimental/theoretical $\bar{\alpha}$ and $\chi^{(1)}$ parameters for the Zn(II) complex with 6-Brpic ligand were calculated at 35.18 × 10⁻²⁴/40.93 × 10⁻²⁴ and 15.20 × 10⁻²/15.98 × 10⁻² esu [16]. It can expressly be seen the effect of strength of electron–accepting (Cl and Br) located at the 6-position, by regarding comparison of these parameters for these Zn(II) complexes.

The first-order hyperpolarizability (β) values for the Zn(II) complex in ethanol and gas phase calculated at 9.50 × 10⁻³⁰ and 3.72 × 10⁻³⁰ esu (with M06-L level) were found to be the higher than that of urea (0.130 × 10⁻³⁰ esu). On the other hand, the β values for the Zn(II) complexes with pic/6-Brpic/6-Mepic ligands in

Table 7

The ground dipole moment (μ_g, in Debye), the mean linear polarizability (‹α›, in 10^{-24} esu), refractive index (n), linear susceptibility ($\chi^{(1)}$, in 10^{-2} esu), anisotropy of linear polarizability ($\Delta\alpha$, in 10^{-24} esu), mean first – and second – order hyperpolarizabilities (‹β› and ‹γ› in 10^{-30} and 10^{-36} esu), and third – order susceptibility ($\chi^{(3)}$, in 10^{-13} esu) for the Zn(II) complex.

Property	M06L		ωB97XD	
	Ethanol	Gas phase	Ethanol	Gas phase
μ	14.24	6.84	15.21	7.45
μ^a	6.20			
‹α›	40.93	30.57	39.52	29.68
‹α_{exp}›	25.83			
‹α›^{a}	17			
$\Delta\alpha$	10.23	8.98	11.40	8.41
n	1.86	1.52	1.75	1.41
n_{exp}	1.49			
$\chi^{(1)}_{calc}$	24.45	17.14	21.91	14.95
$\chi^{(1)}_{exp}$	12.01			
‹β›	9.50	3.72	2.63	1.32
‹β›^{a}	9.2			
‹γ›	84.81	52.53	44.51	38.61
$\chi^{(3)}$	50.58	16.33	20.37	8.94
‹γ›^{a}	15			

^{a} pNA results taken from [89].

ethanol/gas phase were calculated at 0.005×10^{-33} [13], $4.57 \times 10^{-30}/4.21 \times 10^{-30}$ [16] and $1.9 \times 10^{-30}/2.0 \times 10^{-30}$ esu [21], respectively. These results show that it is lower than the non-linear optical characteristic effect exhibited by Zn(II) complex with pic and 6-Clpic ligands. The second-order hypepolarizability (γ) values of the Zn(II) complex in ethanol/gas phase calculated at $84.81 \times 10^{-36}/52.53 \times 10^{-36}$ and $44.51 \times 10^{-36}/38.61 \times 10^{-36}$ esu (with M06-L and ωB97XD levels) were 5.654/3.502 times and 2.967/2.574 times higher than that of pNA (15×10^{-36} esu), respectively. In reported studies on Zn(II), Cu(II) and Co(II) complexes of pyridine derivatives [79,80,91], the experimental $\chi^{(3)}$ values were found to be 6.74×10^{-6} esu for bis(picolinic acetate)Zinc (II), 2.00×10^{-13} esu for [Cu$_2$(pydc)$_2$(inta)$_2$(H$_2$O)$_2$]·3H$_2$O. In the present work, when the theoretical $\chi^{(3)}$ values obtained at 50.58×10^{-13} and 20.37×10^{-13} esu are compared with the reported Zn(II) complexes with 6-Mepic/6-Brpic ligands, the present results exhibit that the powerful indicator of the microscopic third-NLO activity. These differences can originate from the coordination geometry, around the metal ion and electron density transfer within the molecular system.

By considering NLO results, it could be stated that the Zn(II) complex could be an efficient material for microscopic second-order and especially third-order NLO property.

3.6. Concentration effects on the optical and the electrical conductivity

The optical conductivity (σ_{opt}) and electrical conductivity (σ_{elec}) depending on light velocity (c), refractive index (n) and absorption coefficient (α) displaying importance for optical materials and devices are calculated by eq. (23) and (24) [92,93],

$$\sigma_{opt} = \frac{\alpha n c}{4\pi} \tag{23}$$

$$\sigma_{el} = \frac{\lambda n c}{2\pi} \tag{24}$$

Fig. 11 displays the variations of optical and electrical conductivity versus E of the Zn(II) complex at 13, 33, 44 and 94 μM concentrations in ethanol. From Fig. 11a and 11b, the σ_{opt} values of the Zn(II) complex being in the order of 10^9 s^{-1} are much higher than those of the σ_{elec} values. While the σ_{opt} parameter of the Zn (II) complex do not change until 3.1 eV, it increases in the same

way as depending on the increase in molar concentration in the electronic maximum absorption regions (Fig. 11a). Unlike, the σ_{elec} curves of the Zn(II) complex sharply decrease until 3.1 eV, other parts of the curve show similar trend with the σ_{opt} parameter.

3.7. Concentration effects on dielectric parameters

The complex dielectric constant includes the real part ε_1 and the imaginary part ε_2 described by the eq. (25) and (26) [74,76,80].

$$\varepsilon_1 = n^2 - k^2 \tag{25}$$

$$\varepsilon_2 = 2nk \tag{26}$$

The graphs of the real and imaginary dielectric constant depending on the photon energy are given in Fig. 12a and 12b. By considering on molar concentrations between 3 and 6 eV energy regions, the real and imaginary part of dielectric constant of the Zn (II) complex demonstrate the same trend in accordance with the increase in molar concentrations. As can be clearly seen from the varying molar concentrations of the Zn(II) complex, the real part of the dielectric constant is greater than the imaginary part because the refractive index of the complex is much greater than the extinction coefficient, and at the same time the curves of the real part display the same trend with curves of the refractive index.

The loss factor is obtained by eq. (27) [76,94].

$$\tan\delta = \frac{\varepsilon_2}{\varepsilon_1} \tag{27}$$

Fig. 13a shows the graph of the loss factor of the Zn(II) complex depending on photon energy. The loss factor values at different molar concentrations between the 3 and 6 eV energy regions of the complex show the same trend with increasing molar concentrations. In addition, these factor values are very small, as the ε_2 values of the complex.

The *VELF* and *SELF*, which are defined as volume and surface energy loss functions, are important parameters in terms of their dependence on parts of the dielectric constants. These functions are obtained by using eq. (28) and (29) [76,77].

$$VELF = \frac{\varepsilon_2^2}{\left(\varepsilon_1^2 - \varepsilon_2^2\right)} \tag{28}$$
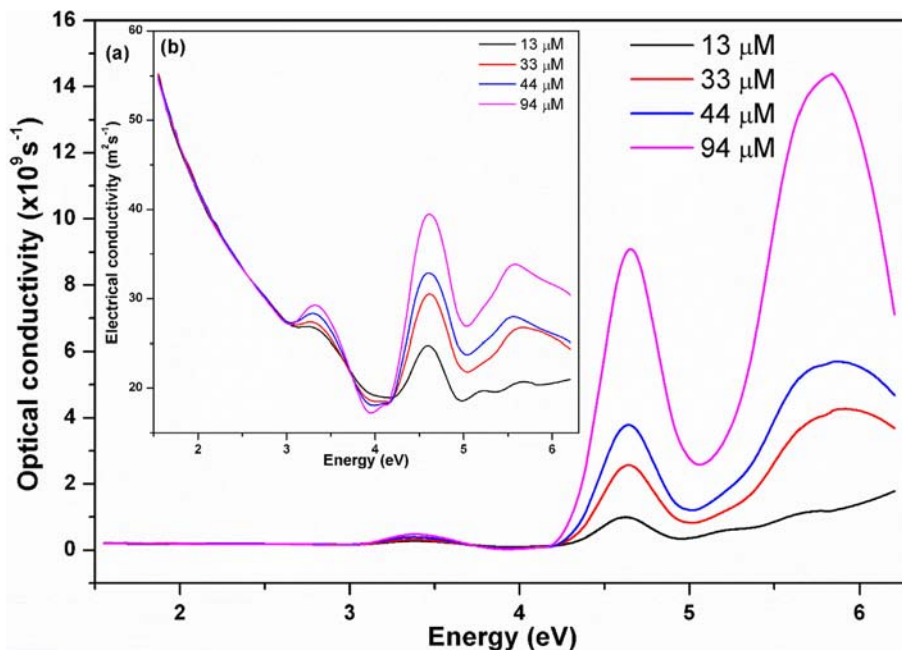
Fig. 11. **(a)** The optical conductivity σ_{opt} and **(b)** the electrical conductivity σ_{elec} vs. *E* of the Zn(II) complex at 13, 33, 44 and 94 μM concentrations in ethanol.
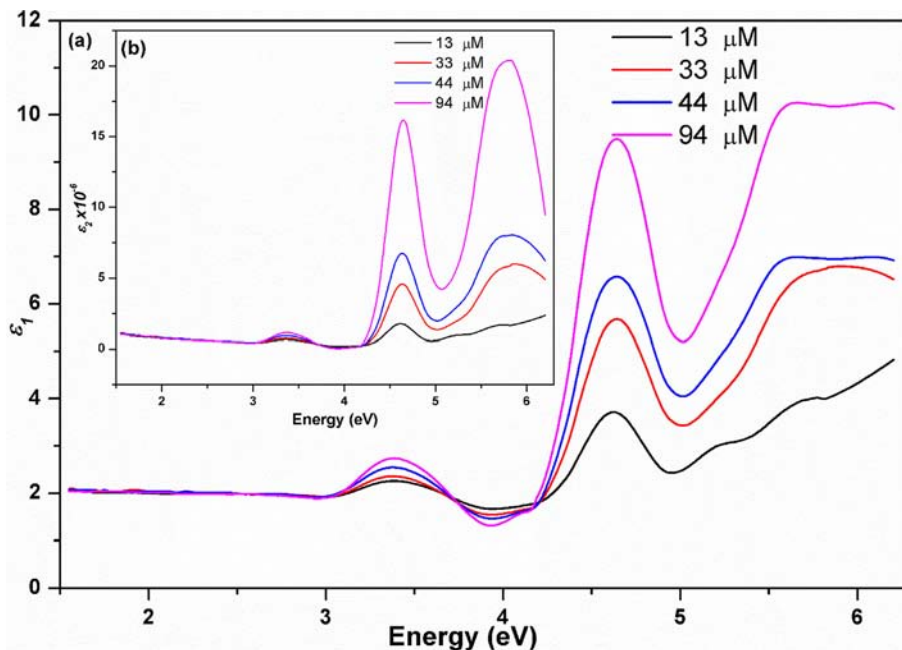

Fig. 12. **(a)** The real part ε_1 and **(b)** the imaginary part ε_2 dielectric spectra of the Zn(II) complex at 13, 33, 44 and 94 μM concentrations in ethanol.

and

$$SELF = \frac{\varepsilon_2^2}{((\varepsilon_1 + 1)^2 + \varepsilon_2^2)} \tag{29}$$

It is clear from the Fig. 13b that the VELF and SELF parameters of the Zn(II) complex exhibit the same trend with increasing in different molar concentrations. VELF values between the 3 and 6 eV energy regions at each molarity were observed greater than SELF values. Fig. 13 shows similar behavior between VELF/SELF and tanδ plots at varying molar constrictions of the complex.

3.8. α Glucosidase assay

The IC$_{50}$ values of the Zn(II) complex, acarbose, genistein and resveratrol [95–98] are presented in Table 8. The IC$_{50}$ values of the [Zn(6-Clpic)(pic)(H$_2$O)$_2$] and [Zn(6-Mepic)$_2$(H$_2$O)]·2H$_2$O against α-glucosidase were found to be 0.44 and 0.46 mM [21], respectively.

From Table 8, the structure–activity relationship (SAR) for the Zn(II) complex can be deduced the follows:

(a) It could be concluded that the coordination environment and metal ions play an important role on α-glucosidase inhibitory activity. In comparison of [Zn(6-Clpic)(pic)(H$_2$O)$_2$] and [Zn(6-
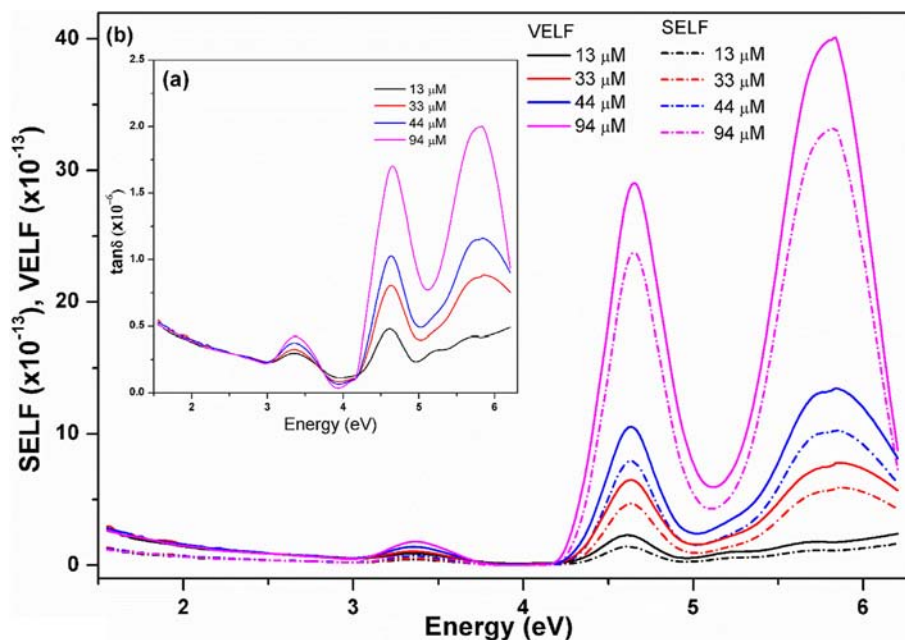
Fig. 13. (a) The loss factor *tanδ* vs. *E* and (b) the volume (VELF) and surface energy loss functions (SELF) vs. *E* of the Zn(II) complex at 13, 33, 44 and 94 μM concentrations in ethanol.

Table 8
In vitro inhibition IC_{50} values (mM) of the Zn(II) complex for α–glucosidase, the protein–ligand interactions and energies.

Compound	IC_{50} (mM)[a]	Z(II) complex-protein interaction	Energy[b] (kcal/mol)
6 – Chloropicolinic acid (6-ClpicH)	not active	Van der Waals interactions	
2 – Picolinic acid (picH)	not active	S[g]–ASN–259	−7.0
[Zn(6-Clpic)(pic)(H₂O)₂]	0.44 ± 0.002	S–ARG–263	−7.8
[Zn(6-mpa)₂(H₂O)]·H₂O[c]	0.46 ± 0.001	M[g]–ILE–272	−6.7
[Co(6-Mepic)(pic)·2H₂O][d]	>0.60	S–ILE–272	−4.1
Genistein	0.008 ± 0.001	S–HIS–295	−6.1
Acarbose[e]	0.91		
Resveratrol[f]	0.01		
		Hydrogen bonding interactions	
		S–ASN–259	−7.0
		S–GLN–260	−2.9
		S–HIS–295	−10.5
		M[g]–SER–298	−3.5
		S–SER–298	−2.5
		E_{total}	−92.8

[a] IC_{50} values represent the means ± S.E.M. of three parallel measurements ($p < 0.05$).
[b] The values of VDW and H – Bond energy are taken as lower than − 4.0 and − 2.5 kcal/mol, respectively.
[c] From ref.[21].
[d] From ref.[99].
[e] From ref.[95,96].
[f] From ref.[97,98].
[g] M and S indicate the main and side chain of the interacting residue, respectively.

Mepic)₂(H₂O)]·2H₂O, the presence of chlorine atom having high electron density on the picolinate ligand increased α-glucosidase inhibitory activity.

(b) The IC_{50} value of the Co(II) complex with 6-Mepic and pic ligands, synthesized in our previous work [99], was found to be > 0.60 mM for α-glucosidase inhibition. It is distinctly observed

that the changing of Co(II) ion and 6-Mepic ligand with Zn(II) ion and 6-Clpic ligand significantly affected on α-glucosidase inhibitory activity.

(c) It could be clearly noted that the different coordination geometries of these complexes having distorted octahedral geometry and trigonal bipyramidal geometry did not display a significant effect on α-glucosidase inhibitory activity.

iGEMDOCK program [69] was applied to determine the interactions of binding site of the target protein (the template structure *S. cerevisiae* isomaltase (PDBID: 3A4A)) with the Zn(II) complex. Table 8 demonstrates the predicted interactions and their energies as well as the IC_{50} values of the Zn(II) complex. The hydrogen bonding and van der Waals interactions between amino-acid residues with the Zn(II) complex are given in Fig. S7. The E_{tot} of the complex obtained at −92.8 kcal/mol contains the interactions of the amino-acid residues with the Zn(II) complex. The H-bonding interaction energy values between carbonyl oxygen atom of picolinate ligand and the S (side chain)-ASN259/HIS295/GLN260 $O^{\delta}/O^{\delta}/O^{\epsilon}$ obtained at 2.91, 3.04 and 3.19 Å bond distances were calculated at −7.0, 10.5 and −2.9 kcal/mol, respectively. Moreover, these interactions for 6-chloropicolinate ligand were considered between carbonyl oxygen atom of 6-Clpic ligand and the M (main chain)/S-SER298 N^{α}/O^{γ} obtained at 3.08 and 2.89 Å bond distances, it was concluded that they were computed with low energy values of −3.5 and −2.5 kcal/mol. When the E_{tot} value of [Zn(6-Clpic)(pic)(H₂O)₂] obtained at −92.8 kcal/mol was compared with that of [Zn(6-Mepic)₂(H₂O)]·2H₂O complex reported at −88.4 kcal/mol [21], it could be noted a similar trend observed in the IC_{50} values of these complexes against α-glucosidase. These energies show that [Zn(6-Clpic)(pic)(H₂O)₂] is more stable than [Zn(6-Mepic)₂(H₂O)]·2H₂O in interactions of the binding site of the target protein. These results are coherent with the α-glucosidase inhibitory activity of these complexes. As a result, it can be stated that similarities and differences in van der Waals and hydrogen bond interactions may arise due to different metal ions and coordination environments in complex structures.

Considering the molecular docking study on the inhibition mechanism of glucosidases, it is speculated that hydrolysis may

occur due to the formation of the anhydride moiety between the carbonyl of the Zn (II) complex and the carboxylate group of amino acid residues in the enzyme active site. Furthermore, it is determined that the interactions of hydrogen-bonding and van der Waals among the Zn(II) complex and amino acid residues affect the α-glucosidase inhibition.

4. Conclusions

The vibrational, electronic and optical behaviors of the [Zn(6-Clpic)(pic)(H$_2$O)$_2$] complex, whose structure was determined by XRD technique, were examined by using experimental and theoretical models. The experimental optical susceptibility and band gap, refractive index, linear polarizability as well as optical and the electrical conductivity, dielectric constant obtained from the UV–Vis spectroscopic data at 13, 33, 44 and 94 μM concentrations in ethanol were investigated. From UV–Vis spectroscopic data, it is concluded that the increasing molar concentrations decrease the values of optical parameters of the Zn(II) complex. By regarding experimental and theoretical results, it could be noted a well consistency between theoretical and corresponding experimental results. The IC$_{50}$ values of the [Zn(6-Clpic)(pic)(H$_2$O)$_2$] and [Zn(6-Mepic)$_2$(H$_2$O)]·2H$_2$O against α-glucosidase were found to be 0.44 and 0.46 mM, respectively. It is distinctly observed that the changing of 6-Mepic ligand with 6-Clpic and pic ligands significantly affected on α-glucosidase inhibitory activity. It could be concluded that the coordination environment and metal ions play an important role on α-glucosidase inhibitory activity. It can be stated to show a potent third-order NLO property the χ$^{(3)}$ results of the Zn (II) complex obtained at 50.58 × 10^{-13} and 20.37 × 10^{-13} esu with M06-L level and observed at 206.6 × 10^{-13} and 294.3 × 10^{-13} esu at 94 μM concentration in UV–Vis region. To sum up, the detailed theoretical and experimental structural, spectral and optical properties of the Zn(II) complex were presented comparatively. Besides, it could be stated that the NLO and in vitro results provided leading information for novel pyridine-base metal complexes to be synthesized.

CRediT authorship contribution statement

Necmi Dege: Data curation, Formal analysis, Visualization. **Özgen Özge:** Data curation, Formal analysis, Visualization. **Davut Avcı:** Methodology, Software, Formal analysis, Writing - review & editing. **Adil Başoğlu:** Conceptualization, Formal analysis, Investigation, Methodology, Software. **Fatih Sönmez:** Formal analysis, Investigation. **Mavişe Yaman:** Data curation, Formal analysis. **Ömer Tamer:** Investigation, Software. **Yusuf Atalay:** Methodology, Software. **Belma Zengin Kurt:** Formal analysis.

Declaration of Competing Interest

The authors declare that they have no known competing financial interests or personal relationships that could have appeared to influence the work reported in this paper.

Appendix A. Supplementary material

Supplementary data to this article can be found online at https://doi.org/10.1016/j.saa.2021.120072.

References

[1] M.A.S. Goher, M.A.M. Abu-Youssef, F.A. Mautner, Synthesis, spectral and structural characterization of a monomeric chloro complex of Zinc(II) with picolinic acid, [Zn(C$_5$H$_4$NCO$_2$H)(C$_5$H$_4$NCO$_2$)Cl], Polyhedron 15 (3) (1996) 453–457.

[2] M. Ghadermazi, J. Soleimannejad, S. Sheshmani, M. Shamsipur, M. Ghanbari, M. Eslami, Characterization, crystal structures and solution studies of Zn(II), Cd (II) and Mg(II) complexes obtained from a proton transfer compound including pyridine-2-carboxylic acid and piperazine, J. Iran. Chem. Soc. 9 (2012) 579–589.

[3] L. Croitor, D. Chisca, E.B. Coropceanu, M.S. Fonari, Diaquabis(pyridine-2-carboxylato-κ²N, O)zinc dimethylformamide hemisolvate, Acta Crystallogr. E 69 (2013).

[4] S. Enthaler, X.-F. Wu, M. Weidauer, E. Irran, P. Döhlert, Exploring the coordination chemistry of 2-picolinic acid to zinc and application of the complexes in catalytic oxidation chemistry, Inorg. Chem. Commun. 46 (2014) 320–323.

[5] B.-M. Kukovec, Z. Popović, G. Povlović, Synthesis and characterization of copper(II) complexes with 3-methylpicolinic acid. Crystal and molecular structure of bis(3-methylpicolinato-N, O)(4-picoline)copper(II), J. Coord. Chem. 61 (19) (2008) 3092–3101.

[6] B.-M. Kukovec, Z. Popovic, G. Pavlovic, Copper(II) complexes with 3- and 6-hydroxypicolinic acid. Preparation, structural, spectroscopic and thermal study, Acta Chim. Slov. 55 (2008) 779–787.

[7] B.-M. Kukovec, Z. Popović, Š. Komorsky-Lovrić, V. Vojković, M. Vinković, Synthesis, structural, spectroscopic and thermal characterization of cobalt complexes with 3- and 6-methylpicolinic acid. Voltammetric and spectrophotometric study in solution, Inorg. Chim. Acta 362 (2009) 2704–2714.

[8] E. L-Chruscinska, G. Micera, E. Garribba, Complex Formation in Aqueous Solution and in the Solid State of the Potent Insulin-Enhancing VIVO2+ Compounds Formed by Picolinate and Quinolinate Derivatives, Inorg. Chem. 50 (2011) 883–899.

[9] B.-M. Kukovec, I. Kodrin, V. Vojković, Z. Popović, Synthesis, X-ray structural, IR spectroscopic, thermal and DFT studies of nickel(II) and copper(II) complexes with 3-methylpicolinic acid. UV–Vis spectrophotometric study of complexation in the solution, Polyhedron 52 (2013) 1349–1361.

[10] S. Altürk, D. Avcı, Ö. Tamer, Y. Atalay, O. Şahin, A cobalt(II) complex with 6-methylpicolinate: synthesis, characterization, second- and third-order nonlinear optical properties, and DFT calculations, J. Phys. Chem. Solids 98 (2016) 71–86.

[11] J.W. Lai, C.W. Chan, C.H. Ng, I.H. Ooi, K.W. Tan, M.J. Maah, S.W. Ng, Hydrated and anhydrous forms of copper(II) complex of 3-methylpicolinic acid, and spectroscopic studies of their ROS-inducing and proteasome inhibition, J. Mol. Struct. 1106 (2016) 234–241.

[12] J. Chai, Y. Liu, J. Dong, B. Liu, B. Yang, Synthesis, structure, chemical and bioactivity behavior of eight chromium(III) picolinate derivatives Cr(R-pic)$_3$, Inorg. Chim. Acta 466 (2017) 151–159.

[13] Ö. Tamer, D. Avcı, E. Çelikoğlu, Ö. İdil, Y. Atalay, Crystal growth, structural and spectroscopic characterization, antimicrobial activity, DNA cleavage, molecular docking and density functional theory calculations of Zn(II) complex with 2-pyridinecarboxylic acid, Appl. Organomet. Chem. 32 (2018) e4540.

[14] S. Altürk, D. Avcı, A. Başoğlu, Ö. Tamer, Y. Atalay, N. Dege, Copper(II) complex with 6-methylpyridine-2-carboxyclic acid: Experimental and computational study on the XRD, FT-IR and UV–Vis spectra, refractive index, band gap and NLO parameters, Spectrochim. Acta A 190 (2018) 220–230.

[15] N. Dege, Ö. Tamer, M. Yaman, A. Başoğlu, D. Avcı, Y. Atalay, Crystallographic, spectroscopic, thermal, optical investigations and density functional theory calculations for novel Co(II) and Mn(II) complexes, Appl. Phys. A 127 (2021) 132.

[16] D. Avcı, Y. Saeedi, A. Başoğlu, N. Dege, S. Altürk, Ö. Tamer, Y. Atalay, Novel Mn (II) and Zn(II) complexes of 6-bromopicolinic acid as a potential optical material: Synthesis, spectral characterizations, linear, and nonlinear optical properties and density functional theory calculations, Appl. Organomet. Chem. (2021) e6125 (https://doi.org/10.1002/aoc.6125).

[17] D. Avcı, S. Altürk, F. Sönmez, Ö. Tamer, A. Başoğlu, Y. Atalay, B.Z. Kurt, N. Dege, Three novel Cu(II), Cd(II) and Cr(III) complexes of 6-Methylpyridine-2-carboxylic acid with thiocyanate: Synthesis, crystal structures, DFT calculations, molecular docking and α-Glucosidase inhibition studies, Tetrahedron 74 (2018) 7198–7208.

[18] D. Avcı, S. Altürk, F. Sönmez, Ö. Tamer, A. Başoğlu, Y. Atalay, B.Z. Kurt, N. Dege, A novel series of M(II) complexes of 6-methylpyridine-2-carboxylic acid with 4(5) methylimidazole: Synthesis, crystal structures, α-glucosidase activity, density functional theory calculations and molecular docking, Appl. Organomet. Chem. 33 (2019) e4935.

[19] D. Avcı, S. Altürk, F. Sönmez, Ö. Tamer, A. Başoğlu, Y. Atalay, B. Zengin Kurt, N. Dege, A novel series of mixed-ligand M(II) complexes containing 2,2′-bipyridyl as potent α-glucosidase inhibitor: synthesis, crystal structure, DFT calculations, and molecular docking, JBIC J. Biolog Inorg. Chem. 24 (2019) 747–764.

[20] D. Avcı, S. Altürk, F. Sönmez, Ö. Tamer, A. Başoğlu, Y. Atalay, B. Zengin Kurt, N. Dege, Novel Cu(II), Co(II) and Zn(II) metal complexes with mixed-ligand: Synthesis, crystal structure, α-glucosidase inhibition, DFT calculations, and molecular docking, J. Mol. Struct. 1197 (2019) 645–655.

[21] D. Avcı, S. Altürk, F. Sönmez, Ö. Tamer, A. Başoğlu, Y. Atalay, B.Z. Kurt, N. Dege, Novel metal complexes containing 6-methylpyridine-2-carboxylic acid as potent α-glucosidase inhibitor: synthesis, crystal structures, DFT calculations, and molecular docking, Mol. Divers. 25 (2020) 171–189.

[22] H.-L. Seng, K.-W. Tan, M.J. Maah, S.-W. Ng, R.N.Z.R.A. Rahman, I. Caracelli, C.-H. Ng, Crystal structure, DNA binding studies, nucleolytic property and

topoisomerase I inhibition of zinc complex with 1,10-phenanthroline and 3-methyl-picolinic acid, Biometals 23 (2010) 99–118.

[23] R.R. Pulimamidi, R. Nomula, R. Pallepogu, H. Shaik, Picolinic acid based Cu(II) complexes with heterocyclic bases – crystal structure, DNA binding and cleavage studies, Eur. J. Med. Chem. 79 (2014) 117–127.

[24] Y. Yoshikawa, R. Hirata, H. Yasui, H. Sakurai, Alpha−glucosidase inhibitory effect of anti−diabetic metal ions and their complexes, Biochimie 91 (2009) 1339–1341.

[25] E. Ueda, Y. Yoshikawa, H. Sakurai, Y. Kojima, N.M. Kajiwara, In vitro α-glucosidase inhibitory effect of Zn(II) complex with 6-methyl-2-picolinmethylamide, Chem. Pharm. Bull. 53 (4) (2005) 451–452.

[26] Q.-X.iu Wu, Y. Geng, Y. Liao, X.-Dan Tang, G.-Chun Yang, Z.-Min Su, Theoretical studies of the effect of electron-withdrawing dicyanovinyl group on the electronic and charge-transport properties of fluorene-thiophene oligomers. Theor. Chem. Acc. 131 (2012) 1121.

[27] S. Altürk, Ö. Tamer, D. Avcı, Y. Atalay, Synthesis, spectroscopic characterization, second and third-order nonlinear optical properties, and DFT calculations of a novel Mn(II) complex, J. Organomet. Chem. 797 (2015) 110–119.

[28] F. Castet, V. Rodriguez, J.-L. Pozzo, L. Ducasse, A. Plaquet, B. Champagne, Design and characterization of molecular nonlinear optical switches, Acc. Chem. Res. 46 (2013) 2656–2665.

[29] L.E. Johnson, L.R. Dalton, B.H. Robinson, Optimizing calculations of electronic excitations and relative hyperpolarizabilities of electrooptic chromophores, Acc. Chem. Res. 47 (2014) 3258–3265.

[30] K. Garrett, X.A.S. Vazquez, S.B. Egri, J. Wilmer, L.E. Johnson, B.H. Robinson, C.M. Isborn, Optimum exchange for calculation of excitation energies and hyperpolarizabilities of organic electro-optic chromophores, J. Chem. Theory Comput. 10 (2014) 3821–3831.

[31] R.S. Roy, P.K. Nandi, Exploring bridging effect on first hyperpolarizability, RSC Adv. 5 (2015) 103729–103738.

[32] M.U. Khan, M. Khalid, M. Ibrahim, A.A.C. Braga, M. Safdar, A.A. Al-Saadi, M.R.S.A. Janjua, First Theoretical framework of triphenylamine−dicyanovinylene-based nonlinear optical dyes: structural modification of π-linkers, J. Phys. Chem. C 122 (7) (2018) 4009–4018.

[33] M.U. Khan, M. Ibrahim, M. Khalid, A.A.C. Braga, S. Ahmed, A. Sultan, Prediction of second-order nonlinear optical properties of D–π–A compounds containing novel fluorene derivatives: a promising route to giant hyperpolarizabilities, J. Clust. Sci. 30 (2) (2019) 415–430.

[34] M.R.S.A. Janjua, M. Amin, M. Ali, B. Bashir, M.U. Khan, M.A. Iqbal, W. Guan, L. Yan, Z.-M. Su, A DFT study on the two-dimensional second-order nonlinear optical (NLO) response of terpyridine-substituted hexamolybdates: physical insight on 2D inorganic-organic hybrid functional materials, Eur. J. Inorg. Chem. 2012 (4) (2012) 705–711.

[35] M.R.S.A. Janjua, M.U. Khan, B. Bashir, M.A. Iqbal, Y. Song, S.A.R. Naqvi, Z.A. Khan, Effect of π-conjugation spacer (−C≡C−) on the first hyperpolarizabilities of polymeric chain containing polyoxometalate cluster as a side-chain pendant: A DFT study, Comput. Theor. Chem. 994 (2012) 34–40.

[36] J.-D. Chai, M. Head-Gordon, Long-range corrected hybrid density functionals with damped atom–atom dispersion corrections, Phys. Chem. Chem. Phys. 10 (2008) 6615–6620.

[37] Y. Zhao, D.G. Truhlar, A new local density functional for main-group thermochemistry, transition metal bonding, thermochemical kinetics, and noncovalent interactions, J. Chem. Phys. 125 (2006) 194101–194118.

[38] M. Malik, D. Michalska, Assessment of new DFT methods for predicting vibrational spectra and structure of cisplatin: Which density functional should we choose for studying platinum(II) complexes?, Spectrochim. Acta A 125 (2014) 431–439.

[39] L. Goerigk, A. Hansen, C. Bauer, S. Ehrlich, A. Najibi, S. Grimme, A look at the density functional theory zoo with the advanced GMTKN55 database for general main group thermochemistry, kinetics and noncovalent interactions, Phys. Chem. Chem. Phys. 19 (2017) 32184–32215.

[40] J. Wang, L. Liu, A.K. Wilson, Oxidative cleavage of the β-O-4 linkage of lignin by transition metals: catalytic properties and the performance of density functionals, J. Phys. Chem. A 120 (2016) 737–746.

[41] P. Verma, Z. Varga, J.E.M.N. Klein, C.J. Cramer, L. Que, D.G. Truhlar, Assessment of electronic structure methods for the determination of the ground spin states of Fe(II), Fe(III) and Fe(IV) complexes, Phys. Chem. Chem. Phys. 19 (2017) 13049–13069.

[42] G.M. Sheldrick, SHELXT – integrated space-group and crystal-structure determination, Acta Cryst. A71 (2015) 3–8.

[43] C.F. Macrae, P.R. Edgington, P.McCabe, E. Pidcock, G.P. Shields, R. Taylor,M. Towler, J. van de Streek, Mercury Visualization and Analysis of Crystal Structures, J. Appl. Crystallogr. 39 (2006) 453–457.

[44] A.L. Spek, Structure validation in chemical crystallography, Acta Cryst. D 65 (2009) 148–155.

[45] H. Sun, W.N. Ding, X.T. Song, D. Wang, M.Z. Chen, K.L. Wang, Y.Z. Zhang, P. Yuan, Y. Ma, R.L. Wang, R.H. Dodd, Y.M. Zhang, K. Lu, P. Yu, Bioorg. Med. Chem. Lett. 27 (2017) 3226–3230.

[46] Gaussian 16, Revision C.01, M. J. Frisch, G. W. Trucks, H. B. Schlegel, G. E. Scuseria, M. A. Robb, J. R. Cheeseman, G. Scalmani, V. Barone, G. A. Petersson, H. Nakatsuji, X. Li, M. Caricato, A. V. Marenich, J. Bloino, B. G. Janesko, R. Gomperts, B. Mennucci, H. P. Hratchian, J. V. Ortiz, A. F. Izmaylov, J. L. Sonnenberg, D. Williams-Young, F. Ding, F. Lipparini, F. Egidi, J. Goings, B. Peng, A. Petrone, T. Henderson, D. Ranasinghe, V. G. Zakrzewski, J. Gao, N. Rega, G. Zheng, W. Liang, M. Hada, M. Ehara, K. Toyota, R. Fukuda, J. Hasegawa, M. Ishida, T. Nakajima, Y. Honda, O. Kitao, H. Nakai, T. Vreven, K. Throssell, J. A. Montgomery, Jr., J. E. Peralta, F. Ogliaro, M. J. Bearpark, J. J. Heyd, E. N. Brothers, K. N. Kudin, V. N. Staroverov, T. A. Keith, R. Kobayashi, J. Normand, K. Raghavachari, A. P. Rendell, J. C. Burant, S. S. Iyengar, J. Tomasi, M. Cossi, J. M. Millam, M. Klene, C. Adamo, R. Cammi, J. W. Ochterski, R. L. Martin, K. Morokuma, O. Farkas, J. B. Foresman, and D. J. Fox, Gaussian, Inc., Wallingford CT, 2016.

[47] GaussView, Version 6.1, R. Dennington, T.A. Keith, J.M. Millam, Semichem Inc., Shawnee Mission, KS, 2016.

[48] Y. Zhao, D.G. Truhlar, Comparative DFT study of van der Waals complexes: Rare-gas dimers, alkaline-earth dimers, zinc dimer, and zinc-rare-gas dimers, J. Phys. Chem. 110 (2006) 5121–5129.

[49] J.-D. Chai, M. Head-Gordon, Systematic optimization of long-range corrected hybrid density functionals, J. Chem. Phys. 128 (2008) 084106.

[50] J.-D. Chai, M. Head-Gordon, Long-range corrected hybrid density functionals with damped atom-atom dispersion corrections, Phys. Chem. Chem. Phys. 10 (2008) 6615–6620.

[51] M.J. Frisch, J.A. Pople, J.S. Binkley, Self-consistent molecular orbital methods 25. Supplementary functions for Gaussian basis set, J. Chem. Phys. 80 (1984) 3265–3269.

[52] P.J. Hay, W.R. Wadt, Ab initio effective core potentials for molecular calculations. Potentials for the transition metal atoms Sc to Hg, J. Chem. Phys. 82 (1985) 270–283.

[53] M. H. Jamroz, Vibrational energy distribution analysis VEDA 4, in, Warsaw Poland, 2004.

[54] M.H. Jamróz, Vibrational Energy Distribution Analysis (VEDA): Scopes and limitations, Spectrochim. Acta A 114 (2013) 220–230.

[55] E. Runge, E.K.U. Gross, Density-functional theory for time-dependent systems, Phys. Rev. Lett. 52 (1984) 997–1000.

[56] S. Miertus, E. Scrocco, J. Tomasi, Electrostatic interaction of a solute with a continuum. A direct utilizaion of Ab initiomolecular potentials for the prevision of solvent effects, J. Chem. Phys. 55 (1981) 117–129.

[57] S.I. Gorelsky, SWizard Program, Revision 4.5, University of Ottawa, Ottawa, Canada, 2010, http://www.sg.chem.net/.

[58] E.D. Glendening, A.E. Reed, J.E. Carpenter, F. Weinhold, NBO Version3.1, TCI, University of Wisconsin, Madison, 1998.

[59] A.E. Reed, F. Weinhold, Natural bond orbital analysis of near-Hartree–Fock water dimer, J. Chem. Phys. 78 (1983) 4066–4073.

[60] J.P. Foster, F. Weinhold, Natural hybrid orbitals, J. Am. Chem. Soc. 102 (1980) 7211–7218.

[61] J.L. Oudar, Optical nonlinearities of conjugated molecules. Stilbene derivatives and highly polar aromatic compounds, J. Chem. Phys. 67 (1977) 446–457.

[62] J.L. Oudar, J. Zyss, Relations between microscopic and macroscopic lowest-order optical nonlinearities of molecular crystals with one-or two-dimensional units, Phys. Rev. A 26 (1982) 2028–2048.

[63] Y. Zhang, C.-Y. Zhao, W.-H. Fang, X.-Z. You, Theor. A molecular design view on the first hyperpolarizability of salicylideneaniline derivatives. Chem. Acc. 96 (1997) 129–134.

[64] D. Avcı, The consistency analysis of different semiempirical calculations on second- and third-order nonlinear optical properties of donor–acceptor chromophores containing α-cyan, Spectrochim Acta A 77 (2010) 665–672.

[65] D. Avcı, Second and third-order nonlinear optical properties and molecular parameters of azo chromophores: Semiempirical analysis, Spectrochim. Acta A 82 (2011) 37–43.

[66] D. Avcı, S. Altürk, Ö. Tamer, M. Kuşbazoğlu, Y. Atalay, Solvent effect in implicit/explicit model on FT–IR, ^{1}H, ^{13}C and ^{19}F NMR, UV–vis and fluorescence spectra, linear, second- and third–nonlinear optical parameters of 2–(trifluoromethyl)benzoic acid: Experimental and computational study, J. Mol. Struct. 1143 (2017) 116–126.

[67] W. Yang, R.G. Parr, Hardness, softness, and the fukui function in the electronic theory of metals and catalysis, Proc. Nati. Acad. Sci. USA 82 (1985) 6723–6726.

[68] P.K. Chattaraj, U. Sarkar, D.R. Ro, Electrophilicity Index, Chem. Rev. 106 (6) (2006) 2065–2091.

[69] J.-M. Yang, C.-C. Chen, GEMDOCK: a generic evolutionary method for molecular docking, Proteins 55 (2004) 288–304.

[70] G. Socrates, Infrared and Raman Characteristic Group Frequencies: Tables and Charts, John Wiley & Sons, 2004.

[71] L. Skripnikov, Chemissian: software to analyze spectra, build density maps and molecular orbitals, Version 4 (43) (2016).

[72] S.I. Gorelsky, A.B.P. Lever, The Electronic Structure and Spectra of [Ru (NH₃)₄(LL)]²⁺ (LL = bpy, bpz, bqdi) studied by Density Functional Theory and INDO/S. Charge Transfer Character of Electronic Transitions and their Solvatochromism, Can. J. Anal. Sci. Spectr. 48 (1) (2003) 93–105.

[73] J. Tauc, A. Menth, States in the gap, J. Non Cryst. Solids 8 (1972) 569–585.

[74] I. Şişman, A. Başoğlu, Effect of Se content on the structural, morphological and optical properties of Bi₂Te₃−ySe_y thin films electrodeposited by under potential deposition technique, Mater. Sci. Semicond. Process. 54 (2016) 57.

[75] E. Erdoğan, B. Gündüz, Optoelectronic parameters of TBADN organic molecule: New aspect to solution technique, Opt. Laser Technol. 91 (2017) 130–137.

[76] B. Gündüz, M. Kurban, Photonic, spectroscopic properties and electronic structure of PTCDI-C8 organic nanostructure, Vib. Spectrosc. 96 (2018) 46–51.

[77] A. Adachi, A. Kudo, T. Sakata, The optical and photoelectrochemical properties of electrodeposited CdS and SnS thin films, Bull. Chem. Soc. Jpn. 68 (1995) 3283–3288.

[78] F. Urbach, The long-wavelength edge of photographic sensitivity and of the electronic absorption of solids, Phys. Rev. 92 (1953) 1324.

[79] A.T. Ravichandran, R. Rathika, M. Kumaresavanji, Growth and Z-scan analysis of semi-organic Bis(picolinic acetate) Zinc(II) single crystal for third order NLO applications, J. Mol. Struct. 1224 (2021) 129048.

[80] R.V. Rajana, S. Gowri, N. Manopradha, D.R. Leenaraj, L.K. Joy, D. Sajan, Growth, structural, third order nonlinear optical properties, dielectric properties, conductivity mechanisms and spectroscopic characterization of a luminescent material trans-diaqua-bis(pyridine-2-carboxylato)-cobalt(ii) dihydrate for optoelectronic applications, Opt. Laser Technol. 119 (2019) 105664.

[81] J. Šponer, P. Hobza, DNA base amino groups and their role in molecular interactions: Ab initio and preliminary density functional theory calculations, Int. J. Quant. Chem. 57 (1996) 959–970.

[82] S.R. Gadre, I.H. Shrivastava, Shapes and sizes of molecular anions via topographical analysis of electrostatic potential, J. Chem. Phys. 94 (1991) 4384–4390.

[83] Y. Atalay, A. Başoğlu, D. Avcı, M. Arslan, T. Ozturk, E. Ertas, Determination and analysis of the dispersive optical constants of the 5, 5′, 6, 6′-tetraphenyl-2, 2′-bi ([1, 3] dithiolo [4, 5-b][1, 4] dithiinylidene)–DDQ complex thin film, Physica B Condens. Matter. 403 (200) 1983-1989.

[84] S.H. Wemple, M. DiDomenico Jr., Oxygen-octahedra ferroelectrics. I. Theory of electro-optical and nonlinear optical effects, J. Appl. Phys. 40 (1969) 720–734.

[85] M. Sheik-Bahae, A.A. Said, T.-H. Wei, D.J. Hagan, E.W. Van Stryland, Sensitive measurement of optical nonlinearities using a single beam, IEEE J. Quantum Electron. 26 (1990) 760–769.

[86] Y. Qian, G. Xiao, G. Wang, B. Lin, Y. Cui, Y. Sun, Synthesis and Z-scan measurements of third-order optical nonlinearity in push–pull molecules with dihydroxylethyl amino donor and nitro acceptor, Dyes Pigm. 75 (2007) 218–224.

[87] M.M. El-Nahass, A.A.M. Farag, Structural, optical and dispersion characteristics of nanocrystalline GaN films prepared by MOVPE, Opt. Laser Technol. 44 (2012) 497–503.

[88] M.D. Bharathi, G. Ahila, J. Mohana, G. Chakkaravarthi, G. Anbalagan, Synthesis, crystal structure, growth, optical and third order nonlinear optical studies of 8HQ2C5N single crystal-An efficient third-order nonlinear optical material, Mater. Chem. Phys. 192 (2017) 215–227.

[89] L.-T. Cheng, W. Tam, S.H. Stevenson, G.R. Meredith, G. Rikken, S.R. Marder, Experimental investigations of organic molecular nonlinear optical polarizabilities. 1. Methods and results on benzene and stilbene derivatives, J. Phys. Chem. 95 (1991) 10631–10643.

[90] C. Adant, M. Dupuis, J. Bredas, Ab initio study of the nonlinear optical properties of urea: Electron correlation and dispersion effects, Int. J. Quantum Chem. 56 (1995) 497–507.

[91] L. Wang, L. Duan, D. Xiao, E. Wang, C. Hu, Synthesis of novel copper compounds containing isonicotinic acid and/or 2,6-pyridinedicarboxylic acid: third-order nonlinear optical properties, J. Coord. Chem. 57 (13) (2007) 1079–1087.

[92] E.B. Sas, M. Kurban, B. Gündüz, M. Kurt, Photophysical, spectroscopic properties and electronic structure of BND: Experiment and theory, Synth. Met. 46 (2018) 39–44.

[93] J.O. Akinlami, I.O. Olateju, Reflection coefficient and optical conductivity of gallium nitride GaN, Semicond. Phys. Quantum Electron. Optoelectron. 15 (2012) 281–284.

[94] N.F. Mott, E.A. Davis, Electronic processes in non-crystalline materials, Oxford University Press, Oxford, 2012.

[95] M. Taha, N. Hadiani Ismail, S. Lalani, M. Qaiser Fatmi, Atia-tul-Wahab, S. Siddiqui, K.M. Khan, S. Imran, M. Iqbal Choudhary, Synthesis of novel inhibitors of α-glucosidase based on the benzothiazole skeleton containing benzohydrazide moiety and their molecular docking studies, Eur. J. Med. Chem. 92 (2015) 387-400.

[96] M. Taha, N. Hadiani Ismail, M. Syukri Baharudin, S. Lalani, S. Mehboob, K.M. Khan, S. Yousuf, S. Siddiqui, F. Rahim, M.I. Choudhary, Synthesis crystal structure of 2-methoxybenzoylhydrazones and evaluation of their α-glucosidase and urease inhibition potential, Med. Chem. Res. 24 (2015) 1310–1324.

[97] J.-W. Zheng, L. Ma, Silver(I) complexes of 2,4-dihydroxybenzaldehyde–amino acid Schiff bases-Novel noncompetitive α-glucosidase inhibitors, Bioorg. Med. Chem. Lett. 25 (2015) 2156–2216.

[98] J.-W. Zheng, L. Ma, Metal complexes of anthranilic acid derivatives: A new class of non-competitive α-glucosidase inhibitors, Chin. Chem. Lett. 27 (2016) 627–630.

[99] S. Altürk, D. Avcı, B. Zengin Kurt, Ö. Tamer, A. Başoğlu, F. Sönmez, Y. Atalay, N. Dege, Two new Co (II) complexes of picolinate: synthesis, crystal structure, spectral characterization, α-glucosidase inhibition and TD/DFT study, J Inorg Organomet. Polym Mater 29 (4) (2019) 1265–1279.